

CHEMICAL CONSEQUENCES OF THE C/O RATIO ON HOT JUPITERS: EXAMPLES FROM WASP-12b, COROT-2b, XO-1b, AND HD 189733b

J. I. MOSES

Space Science Institute, 4750 Walnut Street, Suite 205, Boulder, CO, 80301, USA

N. MADHUSUDHAN

Department of Physics and Department of Astronomy, Yale University, New Haven, CT, 06520-8101, USA

C. VISSCHER

Southwest Research Institute, Boulder, CO, 80302, USA

AND

R. S. FREEDMAN

SETI Institute, Mountain View, CA, 94043 and NASA Ames Research Center, Moffett Field, CA, 94035, USA

submitted to Astrophys. J.

ABSTRACT

Motivated by recent spectroscopic evidence for carbon-rich atmospheres on some transiting exoplanets, we investigate the influence of the C/O ratio on the chemistry, composition, and spectra of extrasolar giant planets both from a thermochemical-equilibrium perspective and from consideration of disequilibrium processes like photochemistry and transport-induced quenching. We find that although CO is predicted to be a major atmospheric constituent on hot Jupiters for all C/O ratios, other oxygen-bearing molecules like H₂O and CO₂ are much more abundant when C/O < 1, whereas CH₄, HCN, and C₂H₂ gain significantly in abundance when C/O > 1. Other notable species like N₂ and NH₃ that do not contain carbon or oxygen are relatively unaffected by the C/O ratio. Disequilibrium processes tend to enhance the abundance of CH₄, NH₃, HCN, and C₂H₂ over a wide range of C/O ratios. We compare the results of our models with secondary-eclipse photometric data from the *Spitzer Space Telescope* and conclude that (1) disequilibrium models with C/O ~ 1 are consistent with spectra of WASP-12b, XO-1b, and CoRoT-2b, confirming the possible carbon-rich nature of these planets, (2) spectra from HD 189733b are consistent with C/O ≲ 1, but as the assumed metallicity is increased above solar, the required C/O ratio must increase toward 1 to prevent too much H₂O absorption, (3) species like HCN can have a significant influence on spectral behavior in the 3.6 and 8.0 μm *Spitzer* channels, potentially providing even more opacity than CH₄ when C/O > 1, and (4) the very high CO₂ abundance inferred for HD 189733b from near-infrared observations cannot be explained through equilibrium or disequilibrium chemistry in a hydrogen-dominated atmosphere. We discuss possible formation mechanisms for carbon-rich hot Jupiters, including scenarios in which the accretion of CO-rich, H₂O-poor gas dominates the atmospheric envelope, and scenarios in which the planets accrete carbon-rich solids while migrating through disk regions inward of the snow line. The C/O ratio and bulk atmospheric metallicity provide important clues regarding the formation and evolution of the giant planets.

Subject headings: planetary systems — planets and satellites: atmospheres — planets and satellites: composition — planets and satellites: individual (HD 189733b, WASP-12b, XO-1b, CoRoT-2b) — stars: individual (HD 189733, WASP-12, XO-1, CoRoT-2)

1. INTRODUCTION

Transit and eclipse observations provide a unique means with which to characterize the physical and chemical properties of “hot Jupiter” exoplanet atmospheres (e.g., Seager and Deming 2010). Of particular importance in terms of furthering our understanding of planetary formation and evolution are the constraints on atmospheric composition provided by multi-wavelength photometric and spectral observations of the star-planet system as the transiting planet passes in front of and behind its host star as seen from an observer’s perspective. Transit and eclipse observa-

tions to date have been used to infer the presence of the molecules H₂O, CO, CO₂, and CH₄ in the tropospheres and/or stratospheres of extrasolar giant planets (e.g., Charbonneau et al. 2005, 2008; Burrows et al. 2005, 2007, 2008; Fortney & Marley 2007; Tinetti et al. 2007, 2010; Barman 2007, 2008; Grillmair et al. 2008; Swain et al. 2008a,b, 2009a,b, 2010; Beaulieu et al. 2008, 2010; Snellen et al. 2010a; Madhusudhan & Seager 2009, 2010a, 2011; Madhusudhan et al. 2011a; Madhusudhan 2012; Désert et al. 2009; Knutson et al. 2011; Line et al. 2011b; Lee et al. 2012; Waldmann et al. 2012).

Despite this remarkable feat, several factors can complicate the compositional analyses from transit and eclipse observations, and the results regarding molec-

ular abundances are typically model dependent. For example, in addition to being sensitive to the atmospheric composition, the transit and eclipse signatures are strongly affected by the atmospheric thermal structure, the presence of clouds and hazes, the efficiency of atmospheric dynamics, and the atmospheric mean molecular mass, bulk metallicity, and elemental ratios (e.g., Seager and Deming 2010). The complexity of the problem is best attacked through a combination of sophisticated theoretical modeling and careful data analysis (e.g., see Marley et al. 2007; Burrows & Orton 2010; Showman et al. 2010; Seager and Deming 2010; Winn 2010, and references therein), but degeneracies between solutions, and resulting uncertainties in composition, will continue to plague the determination of constituent abundances until higher-spectral-resolution observations become available to more unambiguously identify atmospheric species.

The largest source of degeneracy arises from uncertainties in the atmospheric thermal structure and composition. To get around this problem, one can attempt to derive simultaneous constraints on both the composition and thermal structure through statistical treatments that systematically compare millions of forward models with the observed photometric and spectral data (Madhusudhan & Seager 2009) or through parameter estimation and retrieval methods (Madhusudhan & Seager 2010a, 2011; Madhusudhan et al. 2011a; Lee et al. 2012; Line et al. 2011b). Potential drawbacks to these techniques are the necessary treatment of a three-dimensional (3D) system as a one-dimensional (1D) problem and the adoption of some built-in assumptions, such as the presence and extinction characteristics of any clouds/hazes, or the selection of a limited number of molecules that are presumed to contribute to the observed behavior. Moreover, the best mathematical solution may not necessarily make physical sense. As an example, Madhusudhan & Seager (2009), Lee et al. (2012), and Line et al. (2011b) all derive an unexpectedly large CO₂ abundance for HD 189733b based on the dayside eclipse *Hubble Space Telescope* (HST) NICMOS data of Swain et al. (2009a) that so far defies theoretical explanation, even when disequilibrium processes are considered (see Moses et al. 2011; Line et al. 2010). It is not clear at the moment whether the theoretical models are at fault (e.g., they could be missing some key mechanisms that enhance photochemical production of CO₂) or whether there are some problems with the data and/or analysis (e.g., underestimated systematic error bars for the data, or missing opacity sources for the spectral models). Although these techniques are powerful, it is always a good idea to follow up such studies with physically based forward models to confirm that the derived characteristics can be explained theoretically.

One interesting and surprising result from these and other observational analyses is the suggestion of a low derived water abundance for several of the close-in transiting exoplanets examined to date, in comparison with CO and/or CH₄, or in comparison with expectations based on solar-composition atmospheres in chemical equilibrium. The H₂O abundance has been suggested to be anomalously low on WASP-12b (Madhusudhan et al. 2011a, see also Cowan et al. 2012), and this conclusion seems firm based on model comparisons with the *Spitzer*

Space Telescope dayside eclipse data of Campo et al. (2011). Water has also been reported to be low on HD 189733b (Grillmair et al. 2007; Swain et al. 2009a; Madhusudhan & Seager 2009; Désert et al. 2009; Sing et al. 2009; Line et al. 2011b; Lee et al. 2012), on HD 209458b (Seager et al. 2005; Richardson et al. 2007; Swain et al. 2009b; Madhusudhan & Seager 2009, 2010a), and on XO-1b and CoRoT-2b (Madhusudhan 2012). The interpretation for these latter planets is not definitive given uncertainties in the thermal structure and other model parameters, and given that solutions with solar-like water abundances have been found that provide acceptable fits to the transit and eclipse data for these planets (e.g., Burrows et al. 2005, 2006, 2008; Fortney et al. 2005, 2008a; Fortney & Marley 2007; Barman et al. 2005; Barman 2007, 2008; Tinetti et al. 2007, 2010; Grillmair et al. 2008; Charbonneau et al. 2008; Swain et al. 2008b; Machalek et al. 2008; Madhusudhan & Seager 2009, 2010a; Beaulieu et al. 2010; Knutson et al. 2012). However, because the fit is often improved for the case of lower water abundances (Madhusudhan & Seager 2009, 2010a; Madhusudhan et al. 2011a; Madhusudhan 2012), the suggestion of lower-than-expected H₂O abundance should not be dismissed out of hand.

Water is thermodynamically stable under a wide variety of temperature and pressure conditions expected for hot-Jupiter atmospheres (e.g., Burrows & Sharp 1999; Lodders & Fegley 2002; Hubeny & Burrows 2007; Sharp & Burrows 2007), and due to the large cosmic abundance of oxygen, H₂O is expected to be one of the most abundant molecules on these transiting planets if one assumes solar-like elemental abundances. Although H₂O can be destroyed by ultraviolet photons, photochemical models predict that water will be effectively recycled in hot-Jupiter atmospheres (Moses et al. 2011; Line et al. 2010, 2011a), keeping H₂O abundances close to thermochemical-equilibrium predictions. Extinction from clouds and hazes could help mask the water absorption signatures, but in that case other molecular bands would be affected as well, making the spectrum appear more like a blackbody (e.g., Liou 2002). If the interpretation is robust, one possible explanation could be that the atmospheres are relatively enriched in carbon, with C/O ratios > 1, which leads to small H₂O/CO and H₂O/CH₄ ratios in hot-Jupiter atmospheres (Seager et al. 2005; Kuchner & Seager 2005; Fortney 2005; Lodders 2010; Madhusudhan et al. 2011a,b; Madhusudhan 2012; Kopparapu et al. 2012).

The influence of elemental abundances such as the bulk C/O and C/N ratios on exoplanet composition and spectra has not been as well studied as some of the other factors that can affect the observations — investigators tend to simply assume solar-like elemental ratios in their models. This neglect is unfortunate, as giant planets can conceivably have elemental compositions different from their host stars, and the atmospheric C/O ratio can provide a particularly important clue for unraveling the formation and evolutionary history of the planets (e.g., Lunine et al. 2004; Owen & Encrenaz 2006; Johnson & Estrada 2009; Mousis et al. 2011; Madhusudhan et al. 2011b; Öberg et al. 2011). The C/O ratio in a giant planet’s atmosphere will reflect not only

the composition of the circumstellar disk in which the planet formed, but physical properties of the disk (such as the total disk mass and temperature structure), the planet’s formation location within the disk (especially in relation to various condensation fronts), the rate of planet formation, and the evolutionary history of the planet and disk, including migration history and relative contribution of gas versus solid planetesimals in delivering heavy elements to the atmosphere.

Regardless of whether the planet formed and remained beyond what was once a putative “snow line” in the disk, like our own solar-system giant planets, or whether it migrated from behind the snow line or from elsewhere in the disk to its present short-period orbital positions, like the close-in transiting hot Jupiters, the C/O ratio can help unravel the conditions in the protoplanetary disk and the timing, history, and mechanism of the planet’s formation and evolution (e.g., Larimer 1975; Larimer & Bartholomay 1979; Lattimer et al. 1978; Lunine & Stevenson 1985; Stevenson & Lunine 1988; Prinn & Fegley 1989; Lodders & Fegley 1993, 1995, 1999; Niemann et al. 1998; Cyr et al. 1998, 1999; Owen et al. 1999; Atreya et al. 1999; Krot et al. 2000; Gaidos 2000; Gautier et al. 2001; Hersant et al. 2004, 2008; Lodders 2004, 2010; Lunine et al. 2004; Wong et al. 2004; Cuzzi & Zahnle 2004; Cuzzi et al. 2005; Alibert et al. 2005; Kuchner & Seager 2005; Ciesla & Cuzzi 2006; Owen & Encrenaz 2006; Guillot & Hueso 2006; Wooden 2008; Dodson-Robinson et al. 2009; Mousis et al. 2009a,b, 2011; Bond et al. 2010; Madhusudhan et al. 2011b; Madhusudhan 2012; Najita et al. 2011; Öberg et al. 2011; Ebel & Alexander 2011; Kopparapu et al. 2012).

The atmospheric C/O ratio itself can have a strong influence on the relative abundance of the spectroscopically important H₂O, CH₄, CO, CO₂, C₂H₂, and HCN molecules (Lodders & Fegley 2002; Seager et al. 2005; Kuchner & Seager 2005; Zahnle et al. 2009a; Madhusudhan & Seager 2010a; Lodders 2010; Line et al. 2010; Madhusudhan et al. 2011a; Madhusudhan 2012; Kopparapu et al. 2012). A photospheric value of C/O \approx 0.55 seems to be the consensus for our Sun, despite some disagreement over the exact absolute C/H and O/H ratios (Allende Prieto et al. 2001, 2002; Asplund et al. 2005, 2009; Grevesse et al. 2007, 2010; Caffau et al. 2008, 2010; Lodders et al. 2009), but possible departures from the canonical solar value or from the host-star’s value need to be considered in atmospheric models.

This need is spotlighted by the low derived H₂O abundances for some exoplanets mentioned above, and in particular, by the recent inference of a carbon-rich atmosphere for WASP-12b (Madhusudhan et al. 2011a). In fact, Madhusudhan (2012) and Madhusudhan et al. (2011b) suggest that super-solar C/O ratios could potentially explain not only the unusual eclipse photometric band ratios of several transiting exoplanets (e.g., WASP-12b, WASP-14b, WASP-19b, WASP-33b, XO-1b, CoRoT-2b), but also the lack of an apparent thermal inversion in some highly irradiated hot Jupiters, due to the fact that TiO — one candidate absorber that could cause a stratospheric thermal inversion (Hubeny et al. 2003; Fortney et al. 2006b; Burrows et al.

2006) — does not form in significant quantities when atmospheric C/O ratios \gtrsim 1. To provide a good fit to the secondary-eclipse data, the carbon-rich models identified by Madhusudhan et al. (2011a) and Madhusudhan (2012) all require specific constraints on species abundances and thermal profiles, and it remains to be demonstrated that the derived abundances make sense from a disequilibrium-chemistry standpoint.

We therefore develop equilibrium and disequilibrium models to better quantify the effects of the C/O ratio on exoplanet atmospheric composition in a general sense, as well as to specifically check whether the molecular abundances derived from analyses such as Madhusudhan & Seager (2009, 2010a, 2011), Madhusudhan et al. (2011a), Madhusudhan (2012), Lee et al. (2012), and Line et al. (2011b) are physically and chemically plausible for assumptions of either equilibrium or disequilibrium conditions. We will also check whether additional molecules that are typically not considered in spectral models could be contributing to the observed behavior of transiting hot Jupiters. Our disequilibrium models include the effects of thermochemical and photochemical kinetics and vertical transport in controlling the vertical profiles for the major neutral carbon, nitrogen, and oxygen species through the entire relevant atmospheric column, from the equilibrium-dominated deep troposphere up through the quench regions for the major species, and on up to the photochemistry-dominated upper stratosphere (Visscher et al. 2010b; Moses et al. 2010, 2011; Visscher & Moses 2011). Differences that occur as a result of the C/O ratio will be highlighted.

2. MODELS

We restrict our study to C-, N-, and O-bearing species (along with H and He) because these are the most cosmically abundant of the reactive heavy elements, because they will be incorporated into the most abundant and most spectrally significant molecules in the infrared photospheres of hot Jupiters, and because their kinetic behavior is better understood than that of other elements like sulfur, phosphorus, alkalis, halides, or metals. The chemistry of other elements will be interesting in its own right, but given the lower cosmic abundances of these elements, their coupled chemistry with C-, N-, and O-bearing compounds is not expected to have a significant impact on the molecular abundances predicted here. One exception is the loss of \sim 20% of the oxygen if the planet is cool enough for silicate condensation to occur (Lodders 2010), and we account for that loss in our model.

We focus on transiting planets that are hot enough that CO rather than CH₄ is expected to be the dominant carrier of atmospheric carbon because the composition of these warmer planets is expected to be more sensitive to changes in the C/O ratio (Madhusudhan 2012). We ignore planets with well-defined stratospheric thermal inversions because we assume (perhaps naively; see Knutson et al. 2010) that TiO is responsible for upper-atmospheric heating (e.g., Hubeny et al. 2003; Fortney et al. 2006b, 2008a; Burrows et al. 2006, 2007, 2008), and thus these planets may be expected to have solar-like C/O ratios (Madhusudhan et al. 2011b). The disequilibrium chemistry of such planets has already been explored (e.g., Moses et al. 2011; Line et al. 2010;

Zahnle et al. 2009b; Liang et al. 2004, 2003).

For our equilibrium calculations, we use the NASA CEA code developed by Gordon & McBride (1994), with thermodynamic parameters adapted from Gurvich et al. (1989-1994), the JANAF tables (Chase 1998), Burcat & Ruscic (2005), and other literature sources. For the disequilibrium calculations, we use the Caltech/JPL 1D photochemistry/diffusion code KINETICS (Allen et al. 1981) to solve the coupled continuity equations that control the vertical distributions of tropospheric and stratospheric species in the case of incident UV irradiation (e.g., Yung et al. 1984; Gladstone et al. 1996; Moses et al. 2000a,b, 2005, 2010, 2011; Liang et al. 2003, 2004; Line et al. 2010, 2011a; Visscher et al. 2010b; Visscher & Moses 2011).

2.1. Photochemical and Thermochemical Kinetics and Transport Model

When transport time scales are shorter than chemical kinetics time scales, the atmospheric composition can depart from strict thermodynamic equilibrium (e.g., Prinn & Barshay 1977; Lewis & Fegley 1984; Visscher & Moses 2011), making thermochemical equilibrium assumptions no longer valid for spectroscopic modeling. This so-called “transport-induced quenching” disequilibrium mechanism will affect the observed composition. The consequences for extrasolar giant planets have been explored by Lodders & Fegley (2002), Cooper & Showman (2006), Visscher et al. (2006), Fortney et al. (2006a), Hubeny & Burrows (2007), Line et al. (2010, 2011a), Moses et al. (2011), Visscher & Moses (2011), and Madhusudhan & Seager (2011). The atmospheric composition can also be altered by the intense ultraviolet radiation from the host star. Absorption of UV photons by atmospheric species can lead to dissociation of the molecules, and the resulting species can react to form new disequilibrium constituents. Models of the photochemistry of transiting hot Jupiters have been presented by Liang et al. (2003, 2004), Yelle (2004), García Muñoz (2007), Koskinen et al. (2007), Zahnle et al. (2009a,b), Line et al. (2010, 2011a), Moses et al. (2011), Miller-Ricci Kempton et al. (2012), Kopparapu et al. (2012), and Venot et al. (2012). The bottom line from the most recent models is that photochemical processes will affect the composition of the middle atmospheres (i.e., the infrared “photospheres”) of all but the hottest of the hot Jupiters, leading to the removal of some expected species like CH_4 and NH_3 from high altitudes and to the production of some other interesting spectrally active constituents like atomic C, O, N, and molecular HCN, C_2H_2 , and in some instances, CO_2 .

For our disequilibrium models, vertical transport is assumed to occur via molecular and eddy diffusion. The eddy diffusion coefficient K_{zz} , which is a free parameter in our models, provides a measure of the strength of atmospheric mixing via convection, atmospheric waves, and eddies of all scales. Although the vertical winds derived from general-circulation models (GCMs) such as those of Showman et al. (2009) can be used as a guide for defining K_{zz} (see Moses et al. 2011), we simply assume an altitude-independent (constant) value for K_{zz} for the models presented here. We allow the solutions for the vertical species profiles to reach a steady state. The

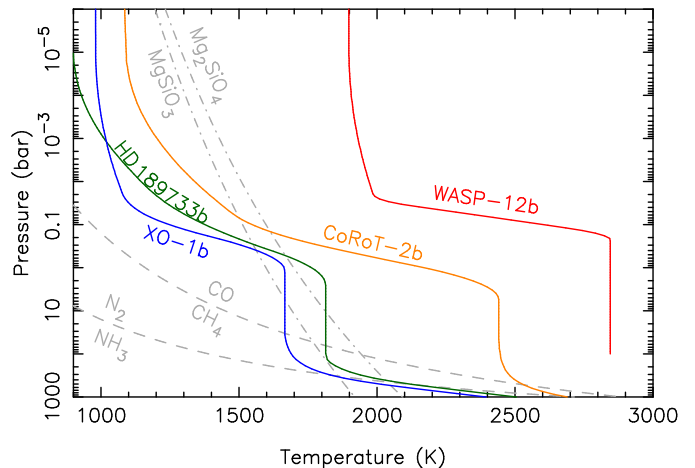


FIG. 1.— Temperature profiles (solid lines, as labeled) adopted for our dayside atmospheres, selected from models presented in Madhusudhan & Seager (2009), Madhusudhan et al. (2011a), and Madhusudhan (2012). The gray dot-dashed lines illustrate the condensation curves for enstatite (MgSiO_3) and forsterite (Mg_2SiO_4), and the gray dashed lines indicate equal-abundance curves for N_2 - NH_3 and CO - CH_4 , all for assumed solar-composition, solar-metallicity atmospheres. The more reduced components (CH_4 and NH_3) dominate to the left of the gray-dashed curves, and the more oxidized species (CO and N_2) dominate to the right. Note that because our solutions do not necessarily favor solar-composition atmospheres, the gray curves will need to be shifted around in response to specific model assumptions; however, CO and N_2 are expected to be the dominant carbon and nitrogen components in the photospheres (a few bar to ~ 0.1 mbar) of all these planets for all our assumed bulk elemental compositions and metallicities. A color version of this figure is available in the online journal.

models all have 198 vertical grid points spaced equally in $\log(\text{pressure})$, typically ranging from the deep troposphere (~ 1 kbar) to well into the thermosphere (pressures $\lesssim 10^{-10}$ bar). The lower boundary is chosen at a hot-enough temperature (typically > 2400 K) to encompass the quench levels for the various major disequilibrium species (e.g., Moses et al. 2011; Visscher & Moses 2011), and the upper boundary is chosen at a high-enough altitude such that the atmosphere is optically thin to the UV radiation that dissociates the key photochemically active species in the model. Note, however, that we do not consider ion chemistry or other processes that are important in the thermosphere and upper stratosphere, and our results at pressures less than ~ 1 μbar should not be taken seriously. For discussions of thermospheric composition and chemistry, see Yelle (2004), García Muñoz (2007), and Koskinen et al. (2010). Plane-parallel geometry is assumed for the radiative calculations in the photochemical model, and multiple Rayleigh scattering by H_2 and He is considered using a Feautrier radiative-transfer method (Michelangeli et al. 1992).

The thermal structure is an input to the KINETICS code; that is, temperatures are not calculated self-consistently. We use specific profiles from the secondary-eclipse analyses of Madhusudhan & Seager (2009, 2010a), Madhusudhan et al. (2011a), and Madhusudhan (2012) to define the thermal structure (see Fig. 1). The dayside hemisphere of the planet contributes to the secondary-eclipse observations, and in fact the hottest regions on the dayside will disproportionately dominate the planetary flux; therefore, our adopted profiles are typically hotter than those derived from 1D radiative-equilibrium models with efficient heat redis-

tribution (e.g., Burrows et al. 2006, 2008; Fortney et al. 2006b, 2010; Barman 2008). In principle, it would seem better to use results from the 3D GCMs to define our thermal structure; however, 3D models are not available for most of the planets we are investigating, and the complexity of the real atmospheres will make it difficult to realistically simulate all the chemical and physical mechanisms that affect the spectrally active molecules and other opacity sources in the GCMs. We therefore rely on the statistical models listed above, which at least satisfy energy balance and provide an adequate reproduction of the observed eclipse data, to define our thermal profiles. Since the quenching of the nitrogen species occurs at high temperatures and pressures deeper in the planet’s troposphere than is accounted for with the thermal profiles of Madhusudhan & Seager (2009, 2010a), Madhusudhan et al. (2011a), and Madhusudhan (2012), we extend these profiles to deeper pressures assuming a somewhat arbitrary adiabat based on the 1D models of Fortney et al. (2008a). At the low-pressure end, we extend the profiles upward nearly isothermally (see Fig. 1). The real upper atmospheres will transition into a high-temperature thermosphere, but Moses et al. (2011) and Line et al. (2011a) demonstrate that the adopted thermospheric structure has little effect on the results for the observable portions of the troposphere and stratosphere. Assuming these fixed temperature-pressure profiles, we then use the hydrostatic equilibrium equation to define the altitude grid.

The reaction list is taken from Moses et al. (2011), and the reader can refer to that paper for further details. The reactions are fully reversed assuming thermodynamic reversibility, which allows the model atmosphere to reach thermochemical equilibrium when kinetic reaction time scales are much shorter than transport time scales. Our nominal $1\times$ solar composition atmospheres assume the protosolar composition from Table 10 of Lodders et al. (2009); however, because our model does not include the rock-forming elements, we assume that 21% of the oxygen is tied up with condensed silicates and metals and is therefore not available for gas-phase chemistry (e.g., Visscher & Fegley 2005; Lodders 2010). Our C/O ratios therefore refer strictly to the gas-phase C/O ratio after any silicate and metal-oxide condensation has occurred and not to the bulk planetary C/O ratio. Note that when we alter the C/O ratio above solar, the oxygen abundance is kept fixed while the carbon abundance is adjusted. Thermochemical equilibrium abundances from the CEA code are used to define the initial species profiles, and zero flux boundary conditions are adopted at the top and bottom boundaries. Again, as discussed in Moses et al. (2011), we expect the atmospheres of these planets to be actively escaping, but our upper boundary condition has no effect on the stratospheric and tropospheric profiles unless the hydrodynamic wind extends down below the thermosphere, at which point our hydrostatic models will be no longer valid.

For the incident stellar ultraviolet flux that drives the photochemistry, we use HST/STIS spectra from epsilon Eri (a K2 V star) and Chi¹ Ori (a G0 V star) from the CoolCAT database (Ayers 2005) for the 1150–2830 Å region to mimic spectra from HD 189733 and WASP-12, respectively, after adjusting for the appropriate distance

scalings. For wavelengths above and below this range, we scale the solar spectrum to match the expected magnitude of the flux for the appropriate stellar type and orbital distance. For XO-1b and CoRoT-2b, we simply adopt the solar spectrum, adjusted to the appropriate orbital distance. The stellar zenith angle is fixed at 48°, which is appropriate for secondary-eclipse conditions (Moses et al. 2011).

2.2. Spectral Models

Given the atmospheric thermal and chemical profiles, as described above for each planet under consideration (namely XO-1b, HD 189733b, CoRoT-2b, and WASP-12b), we use a radiative transfer code to generate a corresponding model spectrum for comparison with observations. We compute emergent thermal spectra using the exoplanetary atmospheric modeling program of Madhusudhan & Seager (2009). The code computes 1D line-by-line radiative transfer in a plane-parallel atmosphere under the assumptions of local thermodynamic equilibrium (LTE) and hydrostatic equilibrium. Line-by-line molecular absorption due to H₂O, CO, CH₄, CO₂, NH₃, C₂H₂, HCN, and H₂-H₂ collision-induced absorption (CIA) is considered. The molecular linelists for H₂O, CO, CH₄, and NH₃ are obtained from Freedman et al. (2008) and references therein, and the HITRAN database (Rothman et al. 2005, 2009). The linelists for CO₂, C₂H₂, and HCN are obtained from Wattson & Rothman (1986), Rothman et al. (2005), and Harris et al. (2008), respectively. The CIA opacities are obtained from Borysow et al. (1997) and Borysow (2002). The emergent spectrum is calculated assuming the planet is at secondary eclipse, i.e. that the integrated flux from the entire dayside atmosphere of the is observed. In order to compute planet-star flux ratios, a Kurucz model spectrum (Castelli & Kurucz 2004) is adopted for the given stellar parameters. While comparing our models with observations of a given planet, we integrate the model spectra over the instrumental bandpasses for which data are available for that system and compute a goodness of fit (e.g., Madhusudhan & Seager 2009; Madhusudhan et al. 2011a).

3. RESULTS

Assuming a “nominal” temperature-pressure profile selected for each of the exoplanets under consideration (see Fig. 1), we investigate how the atmospheric chemistry changes for different assumptions of the atmospheric C/O ratio and metallicity. We first calculate thermochemical equilibrium constituent abundances as a function of pressure for C/O ratios ranging from 0.1 to 1.9, for a variety of assumed bulk atmospheric metallicities. Then, we select one or more representative models with different metallicities and C/O ratios to investigate possible disequilibrium chemistry in more detail with our thermochemical and photochemical kinetics and transport models. Disequilibrium-model solutions will be presented for carbon-to-oxygen ratios of both solar-like (C/O \sim 0.5) and carbon-rich (C/O \gtrsim 1) atmospheres. We then create synthetic spectra from the model results and compare these with the secondary-eclipse data to determine if we can find disequilibrium model solutions that provide an acceptable fit to the data. Our resulting models will be non-unique. Note that because haze

extinction is more likely to affect the transit observations (due to the long slant path being able to amplify extinction from layers that would otherwise be optically thin in the vertical), we restrict our data comparisons to the secondary-eclipse observations. In addition, because *Spitzer* photometric data are available for all the planets in question, we focus on the *Spitzer* dataset.

For any given metallicity, thermal structure, and finite list of molecules that contribute to the spectral signatures, the abundances of the major gas-phase opacity sources required to fit the secondary-eclipse data are well constrained, and there will be a correspondingly narrow range of C/O ratios (if any) that will produce these desired abundances. However, the best-fit C/O ratio will change for different assumptions about the thermal structure and metallicity. Although we examine a few different scenarios in this study, we do not explore the full range of possible parameter space. Our main goal is to illustrate how the C/O ratio affects the composition of highly irradiated hot Jupiters. Our purpose in developing individual models with acceptable spectral fits is to determine whether atmospheres with chemical abundances that are theoretically consistent with “reasonable” metallicities and thermal structures can be derived that reproduce the observed secondary-eclipse data, and in particular, whether models with high C/O ratios are reasonable for the exoplanets that have been reported to have relatively low H₂O abundances. Although we focus on four specific transiting planets in this paper (XO-1b, HD 189733b, CoRoT-2b, WASP-12b), the planets we have selected span a wide range of apparent dayside temperatures from ~ 1300 - 2900 (Cowan & Agol 2011) and can thus serve as proxies for a variety of hot Jupiters.

3.1. HD 189733b Results

The moderate-temperature exoplanet HD 189733b, discovered by Bouchy et al. (2005), resides in the upper part of the O1 regime of the Madhusudhan (2012) classification scheme, in which the C/O ratio is less than unity (as is favored from statistical analyses of the HD 189733b observational data; Madhusudhan & Seager 2009), and temperatures are warm enough that CO dominates over CH₄ in the observable portion of the atmosphere (see Fig. 1), yet temperatures are cool enough that Ti will be tied up in condensates rather than as gas-phase TiO. Various analyses suggest that HD 189733b does not have a significant stratospheric thermal inversion (Fortney et al. 2008a; Burrows et al. 2008; Barman 2008; Charbonneau et al. 2008; Grillmair et al. 2008; Swain et al. 2009a; Madhusudhan & Seager 2009; Showman et al. 2009).

3.1.1. HD 189733b Chemistry

Figure 2 illustrates how the thermochemical equilibrium composition of HD 189733b varies as a function of the atmospheric C/O ratio for our assumed nominal dayside thermal structure and an assumed $1\times$ solar metallicity. For a solar-like C/O ratio of ~ 0.5 , CO and H₂O are the most abundant heavy molecules, CO₂ is much less abundant at the $\lesssim 1$ ppm level, CH₄ and NH₃ are well below ppm levels in thermochemical equilibrium at pressures less than 1 bar, and HCN and C₂H₂ are trace constituents in equilibrium such that they would have

no influence on the eclipse spectra. Although transport-induced quenching could lead to CH₄ (and NH₃) mole fractions greater than 1 ppb at pressures less than 1 bar (see Moses et al. 2011; Visscher & Moses 2011), the CH₄ mole fraction is never likely to rival that of CO for solar-like C/O ratios, unless effective eddy diffusion coefficients are greater than 10^{11} cm² s⁻¹ in the CO-CH₄ quench region (Moses et al. 2011; Visscher & Moses 2011). The relatively low derived CH₄ abundances from the transit and eclipse observations (Swain et al. 2008b, 2009a; Madhusudhan & Seager 2009; Lee et al. 2012; Line et al. 2011b) suggest that atmospheric mixing is not that vigorous on HD 189733b (see Visscher & Moses 2011), and CO mole fractions are likely greater than those of CH₄.

On the other hand, when the C/O ratio is greater than unity, Fig. 2 shows that the equilibrium methane abundance can approach or even exceed that of CO; other oxygen-bearing species like H₂O and CO₂ become much less abundant, and previously unimportant carbon-bearing species like HCN and C₂H₂ become abundant enough to influence spectra. At dayside photospheric temperatures and pressures (~ 1800 - 900 K, ~ 1 -to- 10^{-4} bar), CO is a major constituent for all assumed C/O ratios. When $C \approx O$, available carbon and oxygen will bond together to predominantly form CO; when excess O is available (i.e., $C \lesssim O$), the extra O goes into the formation of H₂O, and to a lesser extent CO₂; when excess C is available (i.e., $C \gtrsim O$), the extra C goes into the formation of CH₄, and to a lesser extent HCN and C₂H₂. When the atmospheric C/O ratio is very near unity, small changes in the C/O ratio lead to large changes in the species abundances.

Working solely from the Madhusudhan & Seager (2009) statistical constraints on the ensemble of models that provide the best fit to the HD 189733b *Spitzer* secondary-eclipse data of Knutson et al. (2007, 2009b) and Charbonneau et al. (2008) (see the red horizontal segments in Fig. 2), it is clear that equilibrium models with C/O ratios < 1 will be required to provide a decent fit to the observations. Here we use the $\xi^2 < 1$ constraints from Madhusudhan & Seager (2009), where $\xi^2 = \chi^2/N_{obs}$, with $N_{obs} = 6$ being the number of photometric data points available for the goodness-of-fit calculations. The CH₄ and CO₂ constraints seem to favor low C/O ratios (perhaps even $C/O < 0.1$), whereas the H₂O constraints can be satisfied with higher C/O ratios. In reality, the water abundance has the biggest influence on the spectral behavior. For our nominal temperature profile and an assumed $1\times$ solar metallicity, H₂O mole fractions that fall near $\sim 1\times 10^{-4}$ provide a significantly better fit to the data than mole fractions even a factor of a few away from the middle of the H₂O-constraint range provided by the Madhusudhan & Seager (2009) $\xi^2 < 1$ criterion. It turns out that for a given temperature profile and metallicity, there is a very narrow range of C/O ratios that provides the necessary best-fit H₂O mole fraction. For our assumed conditions, a C/O ratio near 0.9 provides the desired equilibrium water abundance of $\sim 1\times 10^{-4}$. On the other hand, a C/O ratio of ~ 0.9 also implies a CH₄ abundance at the extreme high end of what is allowable by Madhusudhan & Seager (2009), and implies a very low CO₂ abundance that appears to fall well outside the $\xi^2 < 1$ range for CO₂. Keep in

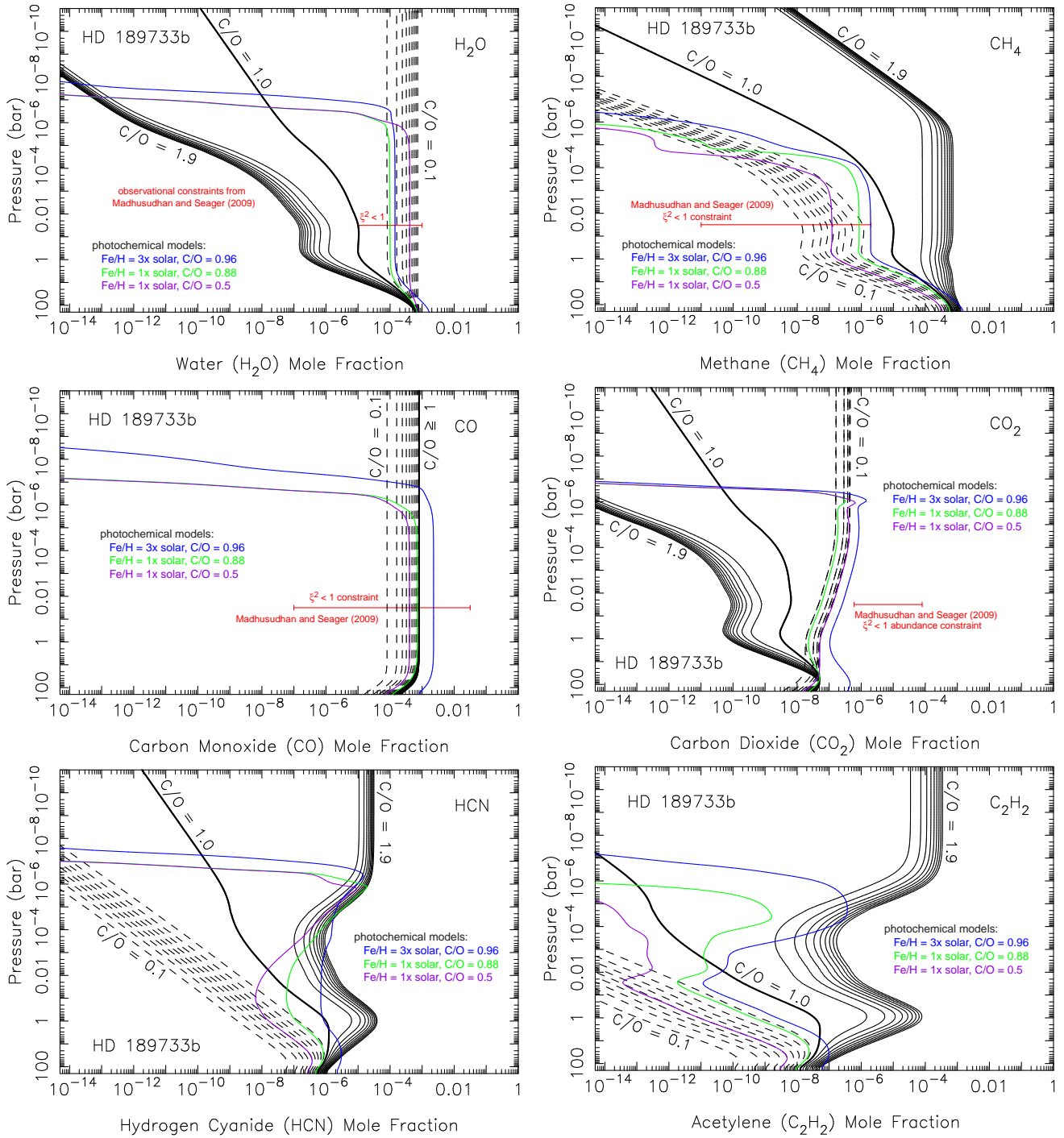


FIG. 2.— Mixing-ratio profiles for H_2O , CH_4 , CO , CO_2 , HCN , and C_2H_2 on HD 189733b from our thermochemical-equilibrium models with assumed $1\times$ solar metallicity but different assumed C/O ratios (ranging from 0.1 to 1.9, incrementing by 0.1 — dashed black lines for $\text{C/O} < 1$, solid lines for $\text{C/O} \geq 1$). The colored lines represent disequilibrium-chemistry results for a model with $1\times$ solar metallicity and a C/O ratio of 0.5 (purple), a model with $1\times$ solar metallicity and a C/O ratio of 0.88 (green), and a model with $3\times$ solar metallicity and a C/O ratio of 0.96 (blue). All disequilibrium models have an assumed moderately-low eddy diffusion coefficient of $K_{zz} = 10^8 \text{ cm}^2 \text{ s}^{-1}$. The horizontal line segments (red) represent the abundance constraints derived by Madhusudhan & Seager (2009) from *Spitzer* IRAC and MIPS observations (Knutson et al. 2007, 2009b; Charbonneau et al. 2008). Note that Madhusudhan & Seager (2009) did not consider HCN and C_2H_2 in their analysis, so abundance constraints for these molecules are not available. A color version of this figure is presented in the online journal.

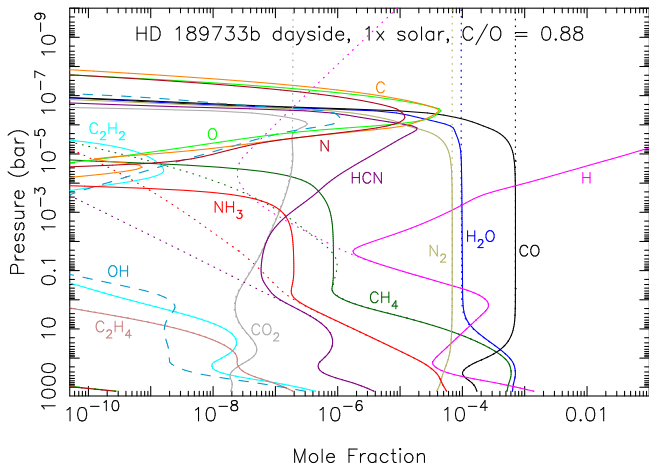


FIG. 3.— Mole-fraction profiles for several important species (as labeled) in a thermochemical and photochemical kinetics and transport model for HD 189733b. Model assumptions include $1\times$ solar metallicity, a C/O ratio of 0.88, and $K_{zz} = 10^8 \text{ cm}^2 \text{ s}^{-1}$ (see also the green curves in Fig. 2). The dotted lines show the thermochemical-equilibrium abundances for the species, using the same color coding. A color version of this figure is available in the online journal.

mind, however, that the CO_2 abundance is essentially unconstrained at the $\xi^2 < 2$ level (Madhusudhan & Seager 2009), and the degeneracy between the contributions of CO and CO_2 in the IRAC channels could be complicating the identification and quantification of the CO_2 abundance.

Can disequilibrium chemistry help improve the comparison with observational constraints? Figure 2 also shows results from a disequilibrium model with an assumed $1\times$ solar metallicity and atmospheric C/O ratio of 0.88 (the green curve). For this model, also shown in Fig. 3, the H_2O abundance essentially follows the chemical equilibrium curve until it reaches high-enough altitudes that molecular diffusion begins to control the profile, at altitudes well above the infrared photosphere (located at a few bars to ~ 0.1 mbar). Photochemistry and transport-induced quenching therefore do not change the favored C/O ratio of ~ 0.9 for a $1\times$ -solar-metallicity atmosphere and our nominal temperature profile. We also find that photochemical production of CO_2 from CO and H_2O chemistry results in little net additional CO_2 , except at very high altitudes, because the CO_2 is able to recycle back to CO and H_2O (see Moses et al. 2011). In this regard, the results from our fully-reversed reaction mechanism are consistent with those of Moses et al. (2011), who find that CO_2 remains in equilibrium with H_2O and CO throughout much of the dayside atmospheric column, in contrast to the results of Line et al. (2010), in which an incompletely reversed reaction mechanism allows CO_2 abundances to be enhanced by a factor of ~ 2 due to photochemistry. Even with a factor-of-two photochemical enhancement, the CO_2 mole fraction would not be large enough in the C/O = 0.88 case to fall within the desired Madhusudhan & Seager (2009) $\xi^2 < 1$ range for CO_2 . For the case of methane, transport-induced quenching slightly enhances the mole fraction as compared with equilibrium in the ~ 1 -to- 10^{-5} bar region, and only above the infrared photosphere do disequilibrium processes reduce the CH_4 abundance; thus, disequilibrium chemistry does not improve the CH_4 abundance

comparisons with regard to the Madhusudhan & Seager (2009) $\xi^2 < 1$ range for methane. Given that water dominates the spectral behavior in the mid-infrared, it may not matter that the other species do not fall precisely within the Madhusudhan & Seager (2009) desired ranges (see Section 3.1.2 below).

The disequilibrium chemistry of HD 189733b with a solar-like atmospheric C/O ratio is discussed extensively in Moses et al. (2011), and we will not repeat that discussion here (see also Line et al. 2010). The main reaction mechanisms controlling the composition are very similar in an atmosphere with C/O = 0.88 versus 0.5, but the resulting abundances can vary significantly between the two cases because of the different equilibrium stabilities. For instance, the water abundance is higher in the C/O = 0.88 model purely because there is more oxygen available once carbon sequesters an amount of oxygen need to form CO, and because photochemical processes do not efficiently remove H_2O and convert it to other oxygen-bearing species. The dominant H_2O recycling mechanism operating in our models is scheme (10) in Moses et al. (2011). Because our nominal thermal structure is warmer than that assumed in Moses et al. (2011) (and our adopted K_{zz} is smaller), our quenched abundances of CH_4 and NH_3 are smaller than in Moses et al. (2011). Note from Fig. 2 that CH_4 quenches at about the same pressure level for both the C/O = 0.88 model (green) and C/O = 0.5 model (purple). The quench point is under the control of reaction scheme (2) of Moses et al. (2011), with $\text{OH} + \text{CH}_3 \rightarrow \text{CH}_2\text{OH} + \text{H}$ being the rate-limiting step for the quenching of $\text{CH}_4 \rightarrow \text{CO}$ conversion under the thermal-structure conditions of our nominal model (see also Visscher & Moses 2011). Because the equilibrium CH_4 abundance is larger at that quench point in the C/O = 0.88 model, the disequilibrium quenched methane abundance is larger with C/O = 0.88 than with C/O = 0.5. The larger quenched methane mole fraction then enhances the effectiveness of mechanisms that convert CH_4 to hydrocarbons like C_2H_2 (see scheme (12) of Moses et al. 2011), and the total column abundance of C_2H_2 through the middle atmosphere is significantly greater for the C/O = 0.88 model.

A similar result occurs for the HCN abundance at low altitudes, but not at high altitudes. Hydrogen cyanide can continue to remain in equilibrium with CO, CH_4 , and NH_3 in the lower and middle stratosphere after these molecules quench. The abundance of molecules that do not contain carbon and oxygen, like NH_3 and N_2 , tend to be relatively unaffected by the C/O ratio. However, because the CO and quenched CH_4 abundances are larger for greater C/O ratios, processes that kinetically convert CO and NH_3 into HCN (see scheme (8) from Moses et al. 2011) or that convert CH_4 and NH_3 into HCN (see schemes (7) and (14) in Moses et al. 2011) are more effective with high C/O ratios than low C/O ratios. That leads to a much larger HCN abundance at low- and mid-stratospheric altitudes above the quench point with the C/O = 0.88 model as compared with the C/O = 0.5 model. However, the upper atmospheric peak abundance of HCN is similar in both models due to the fact that CO and N_2 photochemistry are responsible for the high-altitude production (e.g., see the first scheme in section 3.5 of Moses et al. 2011). High-altitude HCN

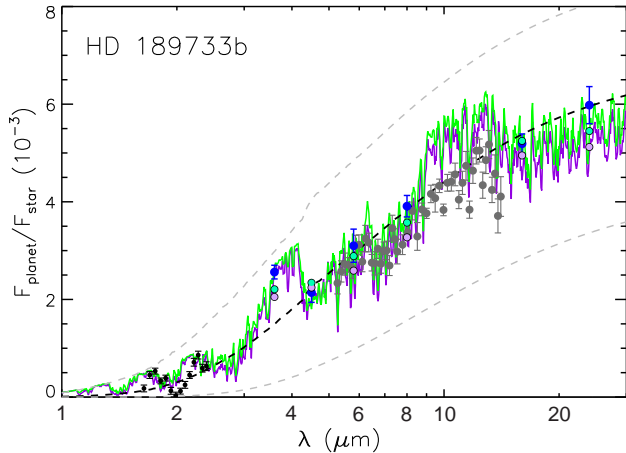


FIG. 4.— Secondary-eclipse spectra for HD 189733b (in terms of the ratio of the flux of the planet to that of the host star). The solid lines represent synthetic spectra from the results of our disequilibrium chemistry models with $1\times$ solar metallicity and $K_{zz} = 10^8 \text{ cm}^2 \text{ s}^{-1}$, for C/O ratios of either 0.88 (green) or 0.5 (purple). The blue circles with error bars represent the *Spitzer* IRAC and MIPS data from Knutson et al. (2007, 2009b) and Charbonneau et al. (2008). The small black circles with error bars represent the HST/NICMOS data of Swain et al. (2009a), and the gray circles with error bars represent the *Spitzer* IRS data of Grillmair et al. (2008). The circles without error bars represent our C/O = 0.88 (green) or C/O = 0.5 (purple) model results convolved over the *Spitzer* IRAC and MIPS instrument response functions. Note the increased absorption for the purple C/O = 0.5 model in all the *Spitzer* channels; the C/O = 0.88 model fits the MIPS and IRAC data better than the C/O = 0.5 model for our particular assumed metallicity and thermal structure. The dashed lines are blackbody curves for assumed temperatures of 900 K (bottom), 1400 K (middle), and 1800 K (top). A color version of this figure is available in the online journal.

production occurs through the reaction $\text{N} + \text{OH} \rightarrow \text{NO} + \text{H}$, followed by $\text{NO} + \text{C} \rightarrow \text{CN} + \text{O}$, followed by $\text{CN} + \text{H}_2 \rightarrow \text{HCN} + \text{H}$. The N and C required for this mechanism are derived from N_2 and CO photolysis. Both these molecules become optically thick to the photolyzing UV radiation (and therefore self shield) at high altitudes, so this mechanism only works within a limited altitude region, but the HCN production rates are substantial. Because the CO and N_2 column abundances at optical depths less than a few are the key defining values for this process to work (which does not change between models), the total production rates from this process are similar in our C/O = 0.5 and C/O = 0.88 models. Hydrogen cyanide is therefore a key photochemical product regardless of the C/O ratio, although the total column above ~ 1 bar will be larger for higher C/O ratios due to the thermochemical kinetics schemes (7), (8), and (14) mentioned in Moses et al. (2011).

In both models, CO and CO_2 track equilibrium profiles because kinetic recycling is efficient, and there are fewer “leaks” into or out of the cycles compared with CH_4 , NH_3 , HCN, and C_2H_x hydrocarbons. The CO recycling is discussed in Moses et al. (2011). Carbon dioxide is recycled through the forward-reverse reaction pair $\text{OH} + \text{CO} \rightleftharpoons \text{CO}_2 + \text{H}$, which is effective throughout the stratosphere for both models. Some net photochemical production for CO_2 does occur at high altitudes, but it does not change the total column abundance in the photosphere.

3.1.2. HD 189733b Spectra

Figure 4 shows synthetic spectra from our disequilibrium models, in comparison with the *Spitzer* IRAC and MIPS secondary-eclipse data for HD 189733b. The plot shows spectra from disequilibrium models with assumed C/O ratios of 0.88 and 0.5 (the green and purple curves from Fig. 2). These two chemical models have identical assumptions other than the C/O ratio. As is obvious from the plots, the model with C/O = 0.88 provides a statistically better fit to the data than the more solar-like C/O = 0.5 model for our assumed $1\times$ -solar-metallicity atmosphere with our adopted nominal thermal profile (i.e., $\xi^2 < 1.9$ for the C/O = 0.88 model versus $\xi^2 < 5.0$ for the C/O = 0.5 model). It is also apparent from the plot that the fit could have been improved with somewhat less methane (note the excess model absorption at 3.6 and 8.0 microns, where CH_4 contributes opacity) and perhaps more CO_2 (note the fit at 4.5 microns, where CO and CO_2 contribute opacity), as was suggested by the Madhusudhan & Seager (2009) $\xi^2 < 1$ ranges. However, the fit from the disequilibrium chemical model with C/O = 0.88 is within 1.4-sigma in all the *Spitzer* bands, on average, implying that theoretically plausible models with carbon-enhanced atmospheres (compared with the solar C/O ratio) can be consistent with the HD 189733b *Spitzer* secondary-eclipse observations.

It must be kept in mind that the fit is not unique. More solar-like C/O ratios may also be consistent with the data, but in that case, Fig. 4 demonstrates that the atmosphere must be much warmer than we are assuming in our nominal model, as our current combination of thermal structure and its resulting chemically-constrained water abundance in the C/O = 0.5 model leads to too much absorption in many of the *Spitzer* bandpasses. However, our temperatures are already at the maximum of what has been predicted from self-consistent 1D models with no energy redistribution from the dayside (Barman 2008, Burrows et al. 2008; see also Fortney et al. 2006b) or from the dayside-average atmosphere in 3D models (Showman et al. 2009), so there is a limit to how low the C/O ratio can go to fit the data while still maintaining a plausible thermal structure.

The solution also depends on assumptions about atmospheric metallicity. For a fixed thermal structure, different metallicities require a different C/O ratio to maintain the desired H_2O mole fraction to compare well with observations (see Fig. 5). For example, if the atmospheric metallicity were $3\times$ solar, the C/O ratio would need to be ~ 0.96 for the H_2O mole fraction to be near 10^{-4} in equilibrium in the photospheric region of HD 189733b for our nominal thermal structure (see also the disequilibrium model represented by the blue curve in Fig. 2). The greater the metallicity, the closer to unity the C/O ratio must be to remain consistent with the spectral analysis of Madhusudhan & Seager (2009) (i.e., super-solar metallicities tend to require super-solar C/O ratios to remain consistent with observations, for atmospheric temperatures at or below those represented by our nominal thermal profile). For subsolar metallicities, more solar-like C/O ratios could produce the desired H_2O abundance.

As was shown by Madhusudhan (2012), the relative abundance of methane and water is a sensitive indicator of the C/O ratio in hydrogen-dominated atmospheres,

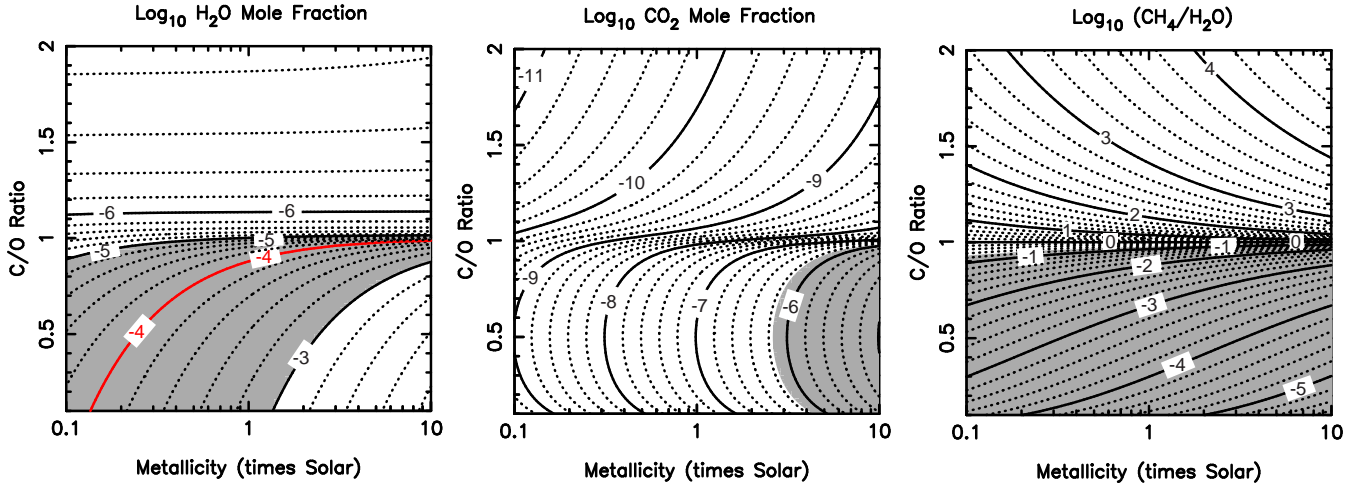


FIG. 5.— The mole fraction of H₂O (Left), CO₂ (Middle), and the CH₄/H₂O ratio (Right) as a function of the C/O ratio and metallicity, assuming thermochemical-equilibrium conditions at 1345 K and 80 mbar (i.e., within the photosphere of our nominal model for HD 189733b). The shaded regions represent the $\xi^2 < 1$ observational constraints from Madhusudhan & Seager (2009). The CH₄/H₂O ratio is very sensitive to the C/O ratio, and the CO₂ and H₂O mole fractions are very sensitive to both the atmospheric metallicity and C/O ratio. The planetary spectrum itself is very sensitive to the water abundance, and the red curve in the figure on the left shows our best-fit H₂O model fraction for our nominal thermal structure. The observations indicate C/O < 1 for HD 189733b, but not all of the observationally allowable phase space is chemically plausible. The higher the atmospheric metallicity, the closer to unity the C/O ratio must be to provide the best fit to the *Spitzer* secondary-eclipse spectra. A color version of this figure is available in the online journal.

particularly when photospheric temperatures are warm enough that CO dominates over methane as the major carbon carrier. A CH₄/H₂O ratio less than unity indicates a C/O ratio less than 1 (see Fig. 5). The Madhusudhan & Seager (2009) analysis firmly suggests a C/O ratio < 1 for HD 189733b; however, just how far below unity the C/O ratio can be to remain consistent with observations depends on metallicity. Figure 5 demonstrates that while CH₄/H₂O ratios < 10⁻⁵ are allowable by the Madhusudhan & Seager (2009) spectral analysis, such values are not physically plausible unless the C/O ratio is strongly subsolar (i.e., < 0.1) and/or metallicities are greatly supersolar.

If the CO₂ abundance were well constrained from observations, one could also constrain the overall atmospheric metallicity due to the well-known sensitivity of CO₂ to metallicity (Fig. 5; see also Lodders & Fegley 2002, Fortney et al. 2005, 2006b, 2008b, Burrows et al. 2006, 2008, Zahnle et al. 2009a, Line et al. 2010, Moses et al. 2011). However, using the 4.5- μ m *Spitzer* channel to constrain the CO₂ abundance could be problematic due to the additional contribution of CO opacity at these wavelengths (Fortney et al. 2010; Madhusudhan & Seager 2009). For example, although our 1 \times solar, C/O = 0.88, disequilibrium model has a CO₂ abundance that falls outside the Madhusudhan & Seager (2009) $\xi^2 < 1$ constraint, the model spectrum has a band-averaged 4.5- μ m flux that falls within 1-sigma of the observed flux, and solar metallicities are still plausible for HD 189733b, at least as far as the *Spitzer* secondary-eclipse data are concerned. In fact, Fig. 5 demonstrates that there is not much overlap in the solutions that are consistent with the Madhusudhan & Seager (2009) CO₂ and H₂O $\xi^2 < 1$ constraints in terms of metallicity vs. C/O ratio phase space, and we consider the H₂O abundance to be the more reliable constraint, as water has a larger effect on the spectrum.

The bottom line from our modeling is that although

the *Spitzer*/IRAC secondary-eclipse observations indicate that the C/O ratio is likely less than unity on HD 189733b (see Madhusudhan & Seager 2009), atmospheric models with C/O ratios moderately enhanced over the solar value of ~ 0.55 provide better fits to the *Spitzer* IRAC and MIPS secondary-eclipse data than models with solar-like C/O ratios, given our assumed nominal thermal profile, unless the atmosphere has a subsolar metallicity. More specifically, the flux in the longer-wavelength *Spitzer* bandpasses is very sensitive to the water abundance, and the relatively low H₂O abundance that Madhusudhan & Seager (2009) infer from the secondary-eclipse observations implies low metallicities, high C/O ratios, and/or high dayside temperatures (i.e., very inefficient heat redistribution) on HD 189733b (see also Barman 2008; Burrows et al. 2008).

Disequilibrium processes like photochemistry and transport-induced quenching do not change this conclusion because water is efficiently recycled in the middle atmosphere through photochemical and kinetics processes (see Moses et al. 2011 for more details), although disequilibrium chemistry is found to affect the profiles of other spectrally important molecules such as CH₄, NH₃, and HCN (see Fig. 3 and Line et al. 2010, Moses et al. 2011). We reproduce *Spitzer* secondary-eclipse photometric data well for models with metallicities between 1-5 \times solar and C/O ratios between 0.88-1.0. It should be kept in mind, however, that our fits are non-unique. The C/O ratio that provides the best fit to the observations will depend on both the metallicity and thermal structure, with higher metallicities and/or lower temperatures requiring higher C/O ratios to remain consistent with the data.

3.1.3. HD 189733b Recent Updates

The most recent HD 189733b *Spitzer* IRAC secondary eclipse data of Knutson et al. (2012) imply significantly reduced fluxes in the 3.6 and 4.5 μ m channels (see Fig. 6). With this new data, the derived $F_{\text{planet}}/F_{\text{star}}$ at 3.6- μ m

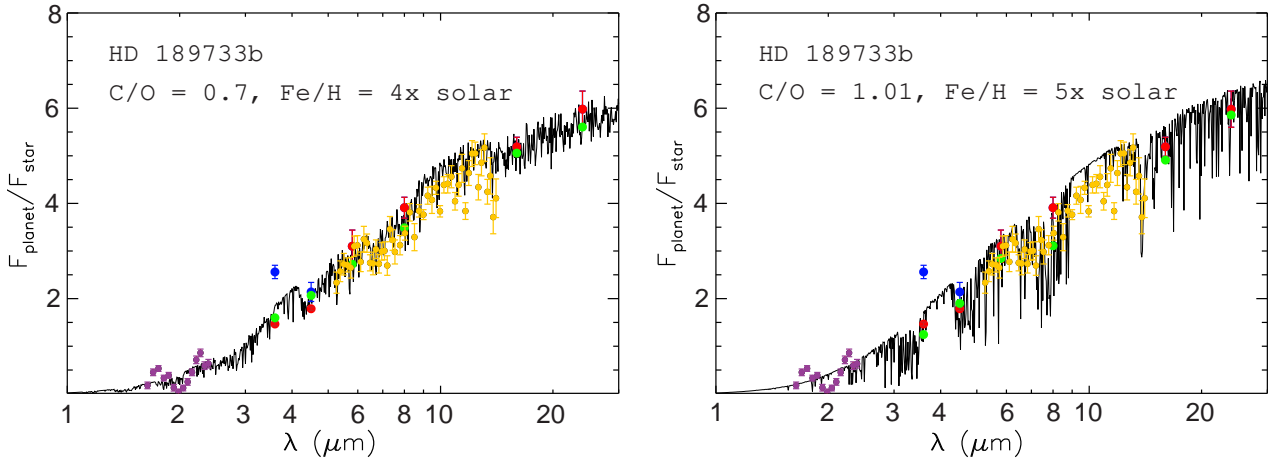


FIG. 6.— Secondary-eclipse spectra for HD 189733b (in terms of the ratio of the flux of the planet to that of the host star) for models with (Left) a C/O ratio of 0.7 and a metallicity of 4 times solar, and (Right) a C/O ratio of 1.01 and a metallicity of 5 times solar. The solid black lines represent synthetic spectra from the results of our disequilibrium chemistry models. The red circles with error bars represent the 3.6 and 4.5 μm *Spitzer* photometric data from Knutson et al. (2012) and the 5.8, 8, 16, and 24 μm data from Knutson et al. (2007, 2009b) and Charbonneau et al. (2008); the blue circles with error bars represent the older data in the 3.6 and 4.5 μm IRAC channels. The purple circles with error bars represent the HST/NICMOS spectra of Swain et al. (2009a), and the yellow circles with error bars represent the *Spitzer* IRS spectra of Grillmair et al. (2008). The green circles without error bars represent our model results convolved over the *Spitzer* instrument response functions. Note that the thermal contrast between the troposphere and stratosphere was reduced in our new models to better fit the new IRAC 3.6 and 4.5 μm points, and the resulting synthetic spectra compare better with the IRS spectra than the older models shown in Fig. 4. A color version of this figure is available in the online journal.

no longer exceeds that at 4.5- μm , and in fact the entire spectrum more closely resembles a blackbody. If the scattering hazes that are observed at ultraviolet and visible wavelengths (e.g., Sing et al. 2011; Huitson et al. 2012) are vertically optically thick at infrared wavelengths, then the spectrum at secondary eclipse might indeed be expected to resemble a blackbody, but a similar result could be obtained with optically thin hazes and less thermal contrast between the stratosphere and troposphere, or from a low-metallicity planet. We have created new models to better fit the new Knutson et al. (2012) 3.6 and 4.5 μm photometric points, along with the older 5.8, 8, 16, and 24 μm data from Knutson et al. (2007, 2009b) and Charbonneau et al. (2008). Some new results are shown in Fig. 6. When we consider models with a reduced ΔT between the troposphere and stratosphere, the predicted model excess-flux “bulges” at 3.5–4 μm and 9–12 μm that were apparent in the previous models shown in Fig. 4 are correspondingly reduced. The new models then compare better with the IRS spectra of Grillmair et al. (2008) and have the appropriate relative fluxes in the 3.6 and 4.5 μm IRAC channels, but the predicted amplitude in the near-IR absorption bands is smaller than is indicated by the HST/NICMOS data of Swain et al. (2009a). As with our previous results, we find that models with moderately high C/O ratios result in the low water abundances that are needed to provide better fits to the data than models with solar-like values of C/O ~ 0.5 ; on the other hand, C/O ratios $\gtrsim 1$ provide too much absorption from methane and HCN at 3.6 and 8 μm to be consistent with the IRAC data. Our favored models have C/O ratios in the range ~ 0.6 –1.0. In all tests, our models provide insufficient absorption at 4.5 μm to account for the Knutson et al. (2012) flux in this channel, considering the exceedingly small statistical error bars cited for the 4.5 μm point. Knutson et al. (2012) had similar difficulty with model fits at 4.5 μm . Increasing the metallicity, with its corresponding increase in the

CO₂ abundance, does not help the situation, as it is still difficult to fit the 4.5- μm point while keeping good fits at other wavelengths. On the other hand, the potential systematic errors involved with the IRAC analyses, the observed variability of the star, and the uncertainties in the stellar models needed for calculating $F_{\text{planet}}/F_{\text{star}}$ for the synthetic spectra all come into play here, and fits such as are shown in Fig. 6 may be reasonable when all systematic observational and modeling uncertainties are considered. In any case, spectral observations by the *James Webb Space Telescope* or dedicated missions like FINESSE and EChO (Swain 2012; Tinetti et al. 2012) could help resolve the atmospheric composition and better constrain the C/O ratio on HD 189733b and other extrasolar planets.

3.2. XO-1b Results

The transiting planet XO-1b was discovered by McCullough et al. (2006). XO-1b, like HD 189733b, is a moderately-irradiated, moderately-hot transiting planet that is warm enough that CO should be the dominant carbon-bearing constituent in the middle atmosphere of the planet. Whether this exoplanet falls into the O1 or C2 regime of Madhusudhan (2012) depends on the C/O ratio. Madhusudhan (2012) suggests that the fit to the *Spitzer*/IRAC secondary-eclipse data of Machalek et al. (2008) is improved for models with C/O ≥ 1 , although Tinetti et al. (2010) are able to find good fits to the same data (as well as to transit data) for more standard assumptions about the C/O ratio, depending on the CH₄ line parameters that are adopted. The relative fluxes in the 3.6 vs. 4.5- μm channels and 5.8 vs. 8.0- μm channels led Machalek et al. (2008) to conclude that XO-1b has a thermal inversion, although their model fit to the data is not very good; Madhusudhan (2012) demonstrates an improved fit for models with no thermal inversion and a C/O ratio ≥ 1 . Tinetti et al. (2010) find a good fit to the secondary-eclipse data for models with and with-

out thermal inversions, for various assumptions about species abundances. For the case of no thermal inversion, the very high flux at $5.8 \mu\text{m}$ implies a very low water abundance and/or very high photospheric temperatures (Tinetti et al. 2010; Madhusudhan 2012). Degeneracies between the thermal structure and composition are clearly plaguing the interpretation of the XO-1b data (e.g., Tinetti et al. 2010; Madhusudhan 2012), and we are unlikely to find a definitive solution to the problem. We can, however, test whether the Madhusudhan (2012) high-C/O-ratio scenarios for XO-1b can fit the secondary-eclipse data for chemically plausible species abundances that take into account disequilibrium processes.

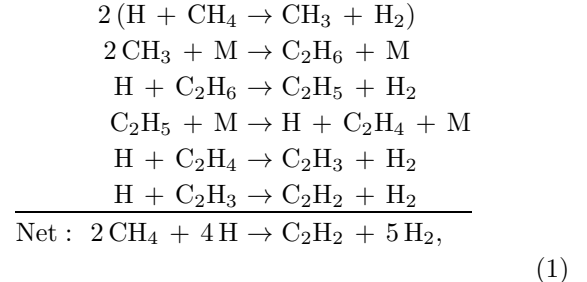
3.2.1. XO-1b Chemistry

Figure 7 illustrates how the thermochemical equilibrium composition of XO-1b varies as a function of the atmospheric C/O ratio for our assumed nominal dayside thermal structure (see Fig. 1) and an assumed $1.5\times$ solar metallicity. As with HD 189733b, CO is abundant for all assumptions of the C/O ratio, whereas H_2O and CO_2 are much more abundant for $\text{C/O} < 1$, and conversely CH_4 , HCN, and C_2H_2 are much more abundant for $\text{C/O} > 1$. The spectral analysis of Madhusudhan (2012) suggests that the C/O ratio on XO-1b could be greater than that on HD 189733b, perhaps even $\text{C/O} > 1$. For a model with a thermal structure similar to our adopted nominal profile shown in Fig. 1, Madhusudhan (2012) finds good fits to the Machalek et al. (2008) *Spitzer* IRAC secondary-eclipse spectra for the species mole fractions marked by a star in Fig. 7. These constraints imply that CO is abundant, CO_2 is much less abundant, and $\text{CH}_4 \gg \text{H}_2\text{O}$. A C/O ratio near unity can satisfy all these constraints for our adopted thermal profile, except the water abundance will be over-predicted for a C/O ratio ~ 1 .

Disequilibrium processes do not affect this overall conclusion much, although the vertical profiles of the spectrally active molecules CH_4 , H_2O , HCN, NH_3 , and CO_2 are significantly altered by transport-induced quenching and photochemistry. The results of three of our thermo/photochemical kinetics and diffusion models are shown in Fig. 7. Further results from one of these disequilibrium models are shown in Fig. 8. The main reaction schemes controlling the abundances in the $\text{C/O} = 0.5$ model are the same as on HD 189733b; a full discussion can be found in Moses et al. (2011) and Line et al. (2010). The disequilibrium processes affecting the molecules do change as C/O exceeds unity, although the main reaction schemes controlling the behavior typically remain the same. The main differences pertain to the relative significance of quenching in controlling the mole fractions of different species in the middle and lower stratosphere, and the different relative abundances of the species at those quench points, which can lead to different “parent” molecules dominating the photochemistry in the upper atmosphere.

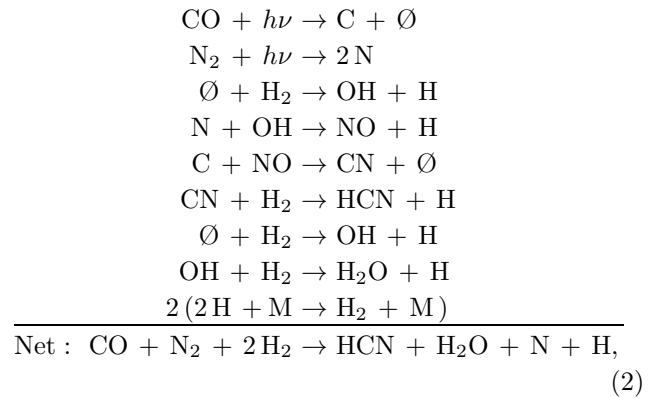
For our favored model with $1.5\times$ solar metallicity, $\text{C/O} = 1.05$, and $K_{zz} = 10^9 \text{ cm}^2 \text{ s}^{-1}$ (Fig. 8), the only molecules relatively unaffected by disequilibrium processes (except at very high altitudes) are CO and N_2 . Compared with equilibrium, photochemistry strongly depletes CH_4 above ~ 0.4 mbar and NH_3 above ~ 1 mbar, although the NH_3 mole fraction in the $1\text{-}10^{-3}$ bar region

is enhanced by transport-induced quenching. Scheme (2) of Moses et al. (2011) still dominates the $\text{CH}_4 \rightarrow \text{CO}$ quenching, but the very high equilibrium CH_4 abundance at the quench point allows methane to be a more important parent molecule for the subsequent photochemistry, with C_2H_2 production in particular being enhanced in the $\text{C/O} = 1.05$ model as compared with the $\text{C/O} = 0.5$ model. The large H abundance in the upper atmosphere drives the conversion of CH_4 into C_2H_2 through schemes such as



where M represents any third body. The key to this mechanism operating in the $\text{CH}_4 \rightarrow \text{C}_2\text{H}_2$ direction is the reaction pair $\text{H} + \text{CH}_4 \rightleftharpoons \text{CH}_3 + \text{H}_2$, which can stay balanced in the lower stratosphere but operates with a net imbalance to the right in the upper stratosphere due to the large abundance of H atoms from H_2O photolysis and subsequent catalytic destruction of H_2 (see Moses et al. 2011).

The greater abundance of CH_4 in the $\text{C/O} = 1.05$ model also leads to significantly enhanced disequilibrium production of HCN in the $\sim 0.1\text{-to-}10^{-4}$ bar region through scheme (7) of Moses et al. (2011). At pressures less than 10^{-4} bar, the HCN is derived from CO and N_2 through schemes such as



where $h\nu$ represents an ultraviolet photon.

Note that photolysis of CO in schemes like the one above leads to the photochemical production of H_2O at high altitudes, despite the low predicted equilibrium abundance of H_2O in this region of the atmosphere in the $\text{C/O} = 1.05$ model. In fact, HCN and H_2O have similar mole fractions at high altitudes in the $\text{C/O} = 1.05$ model because the O from CO photolysis ends up largely as H_2O , whereas the C ends up in HCN. Both H_2O and HCN are recycled efficiently at high altitudes (see Moses et al. 2011). Transport-induced quenching is an important disequilibrium process for water in the $\text{C/O} = 1.05$ model, acting to smooth out the mole-fraction

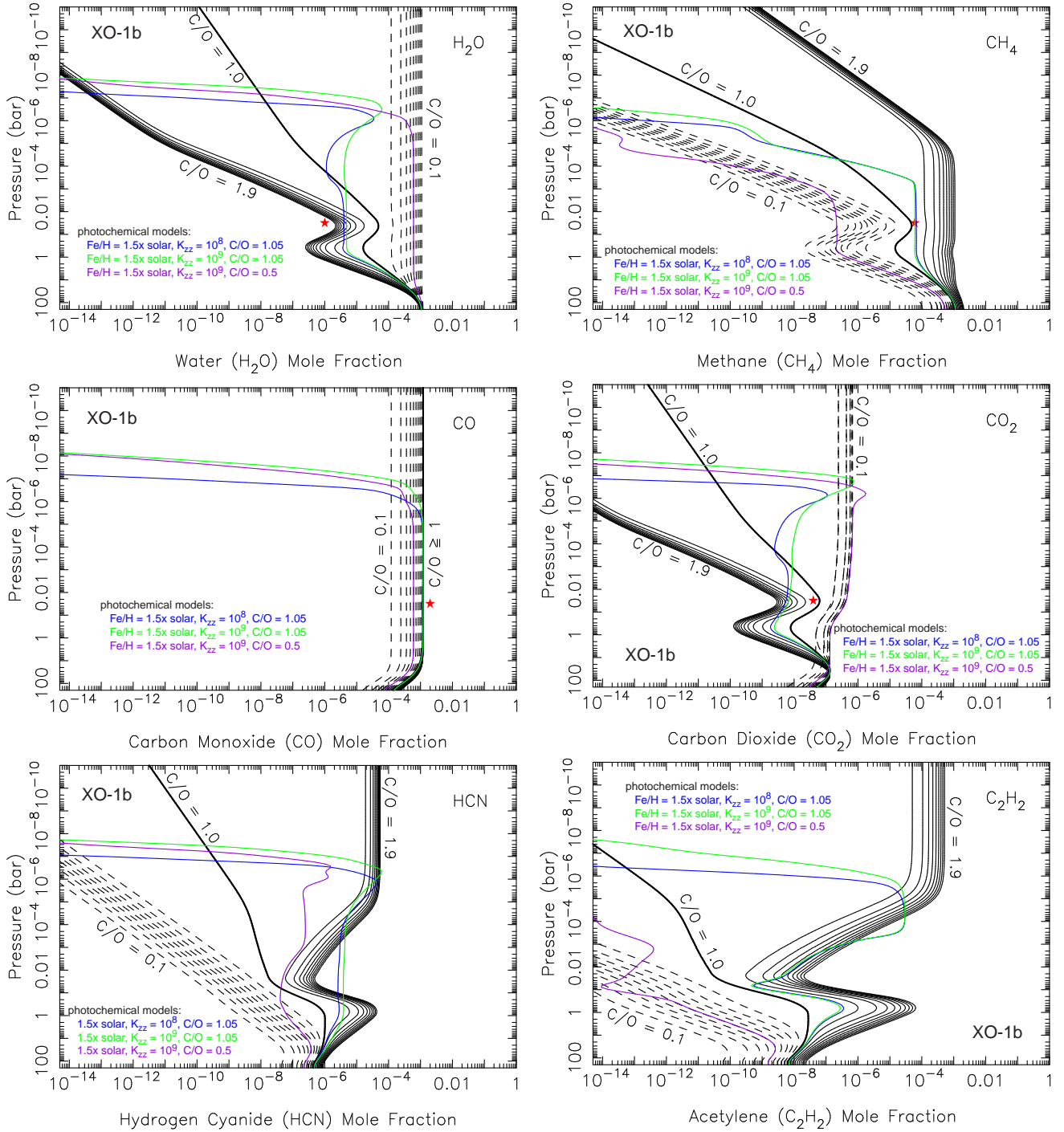


FIG. 7.— Mixing-ratio profiles for H_2O , CH_4 , CO , CO_2 , HCN , and C_2H_2 on XO-1b from our thermochemical-equilibrium models with assumed $1.5\times$ solar metallicity but different assumed C/O ratios (ranging from 0.1 to 1.9, incrementing by 0.1 — dashed black lines for $\text{C/O} < 1$, solid lines for $\text{C/O} \geq 1$). The colored lines represent disequilibrium-chemistry results for models with a solar-like C/O ratio of 0.5 and $K_{zz} = 10^9 \text{ cm}^2 \text{ s}^{-1}$ (purple), a model with a C/O ratio of 1.05 and $K_{zz} = 10^9 \text{ cm}^2 \text{ s}^{-1}$ (green), and a model with a C/O ratio of 1.05 and $K_{zz} = 10^8 \text{ cm}^2 \text{ s}^{-1}$ (blue). All models have an assumed atmospheric metallicity of $1.5\times$ solar. The red stars represent abundance constraints from a model presented in Madhusudhan (2012) based on the *Spitzer*/IRAC secondary-eclipse observations of Machalek et al. (2008); HCN and C_2H_2 were not considered in that analysis. A color version of this figure is presented in the online journal.

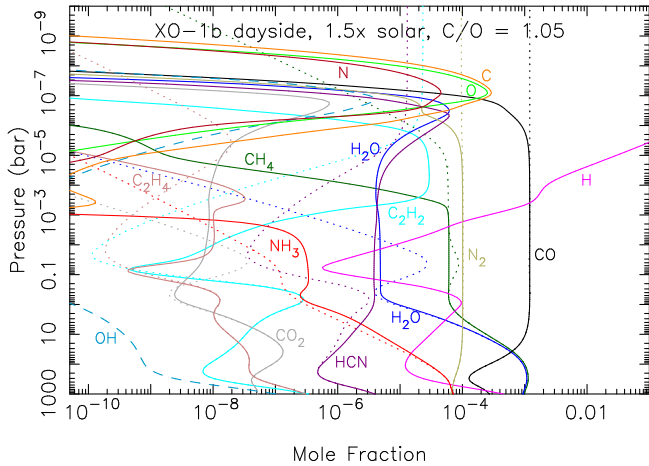


FIG. 8.— Mole-fraction profiles for several important species (as labeled) in a thermochemical and photochemical kinetics and transport model for XO-1b. Model assumptions include $1.5\times$ solar metallicity, a C/O ratio of 1.05, and $K_{zz} = 10^9 \text{ cm}^2 \text{ s}^{-1}$ (see also the green curve in Fig. 7). The dotted lines show the thermochemical-equilibrium abundances for the species, using the same color coding. The overall messiness of this figure indicates that disequilibrium chemistry is important on XO-1b. A color version of this figure is available in the online journal.

profile such that the H_2O abundance drops below equilibrium values near 0.1-0.01 bar but exceeds equilibrium values above $\sim 10^{-2}$ mbar. Quenching of water occurs through the same overall reaction scheme that affects the quenching of CO and CH_4 (e.g., scheme (2) in Moses et al. 2011). This scheme also operates in the $\text{C/O} < 1$ models, but the quenching of water is more obvious in the $\text{C/O} > 1$ models due to the lower equilibrium H_2O abundance. Carbon dioxide is also affected by the quenching of CO and H_2O , and the increased photochemical production of H_2O and OH at high altitudes leads to a significantly increased CO_2 abundance in the $\text{C/O} = 1.05$ model as compared with equilibrium, but the overall abundance of CO_2 remains much lower than that of water.

As with the equilibrium model, the disequilibrium model has more H_2O than the spectral analysis of Madhusudhan (2012) would indicate, but the resulting abundances of CO and CH_4 are still in line with the Madhusudhan (2012) constraints. The disequilibrium models underpredict the CO_2 abundance on XO-1b, as they did for HD 189733b, but again, high CO_2 abundances are not required to fit the thermal-infrared data at secondary eclipse (see below). The disequilibrium models also indicate that hydrogen cyanide is abundant enough that HCN opacity should be included in spectral models.

3.2.2. XO-1b Spectra

In Fig. 9, we compare a synthetic spectrum from our nominal disequilibrium model with the XO-1b *Spitzer* data of Machalek et al. (2008). The photometric data indicate a flux at $4.5 \mu\text{m}$ that is larger than that at $3.6 \mu\text{m}$ and a flux at $5.8 \mu\text{m}$ that is larger than that at $8.0 \mu\text{m}$. In the absence of a thermal inversion, such flux ratios suggest that CH_4 (and/or HCN) are more abundant than H_2O , which is why Madhusudhan (2012) suggested XO-1b could be carbon-rich in the first place. Our spectral fit for this model with $\text{C/O} = 1.05$ is within 1.7-sigma of the data for all the *Spitzer* bands, with the biggest

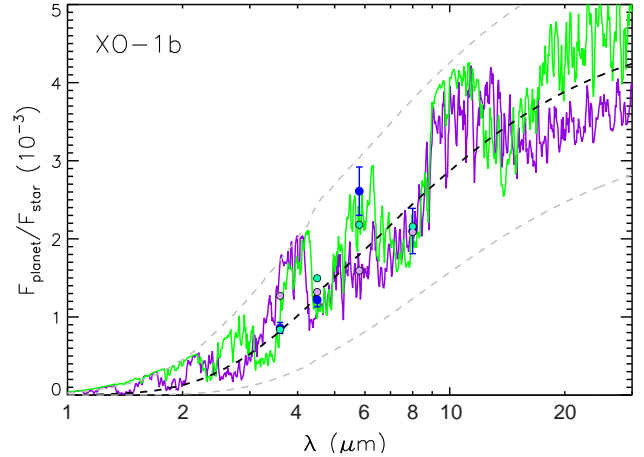


FIG. 9.— Secondary-eclipse spectra for XO-1b. The solid curves represent synthetic spectra from the results of our disequilibrium chemistry models with $1.5\times$ solar metallicity, $K_{zz} = 10^9 \text{ cm}^2 \text{ s}^{-1}$, and C/O ratios of either 1.05 (green) or 0.5 (purple). The blue circles with error bars represent the *Spitzer* IRAC observations of Machalek et al. (2008). The circles without error bars represent the model results for $\text{C/O} = 1.05$ (green) or $\text{C/O} = 0.5$ (purple) convolved over the *Spitzer* bandpasses. Note the much better fit to the data with the $\text{C/O} = 1.05$ model for this particular thermal structure and metallicity. The dashed lines are blackbody curves for assumed temperatures of 900 K (bottom), 1250 K (middle), and 1600 K (top). A color version of this figure is available in the online journal.

problem being an overestimation of the absorption at $5.8 \mu\text{m}$. Going to a higher C/O ratio, with its correspondingly lower water abundance, would improve the fit in this wavelength band, but the resulting larger CH_4 and HCN abundances would degrade the fit at 3.6 and $8.0 \mu\text{m}$. Our spectral comparison here demonstrates that carbon-rich models with plausible species abundances from disequilibrium-chemistry predictions can be consistent with the *Spitzer* secondary-eclipse data, validating the suggestion of Madhusudhan (2012).

Given that XO-1b is cool enough that TiO is not expected to be present in significant quantities in the stratosphere, even for C/O ratios < 1 (and thus TiO would not be available to produce a stratospheric thermal inversion; Hubeny et al. 2003, Fortney et al. 2006b, 2008a), the high C/O-ratio, non-inverted scenario for XO-1b has some theoretical advantages. However, we must again emphasize that our models are not unique. The results will be sensitive to the assumed metallicity and thermal structure, for example. We note that the relative $3.6\text{-}\mu\text{m}/4.5\text{-}\mu\text{m}$ and $5.8\text{-}\mu\text{m}/8.0\text{-}\mu\text{m}$ flux ratios from the XO-1b secondary-eclipse data cannot be explained with solar-like C/O ratios unless temperatures at $\sim 0.1\text{-}1\text{-bar}$ are much hotter ($\gtrsim 2000 \text{ K}$) than is suggested by theoretical predictions or unless the planet has a stratospheric thermal inversion (cf. Machalek et al. 2008; Tinetti et al. 2010). In fact, the observed $5.8\text{-}\mu\text{m}/8.0\text{-}\mu\text{m}$ flux ratio is difficult to explain with any model — whether thermally inverted, anomalously hot at depth, or possessing a high C/O ratio (see Fig. 9, Machalek et al. 2008, Tinetti et al. 2010, Madhusudhan 2012) — and additional high-precision photometric or spectral data from ground-based or space-based observations would be highly desirable in helping constrain chemical and physical properties of this unusual and intriguing exoplanet.

3.3. WASP-12b Results

The transiting planet WASP-12b, discovered by Hebb et al. (2009), is much hotter than either HD 189733b or XO-1b (see Fig. 1). As one of the most highly irradiated hot Jupiters discovered to date, WASP-12b would fall into the upper part of either the O2 or C2 regimes of the Madhusudhan (2012) hot-Jupiter classification scheme, depending on the C/O ratio. WASP-12b is hot enough that titanium would not be cold-trapped into condensed calcium-titanium oxides (e.g., Lodders 2002, 2010) or other condensed phases. Thus, for C/O ratios less than unity, TiO vapor would be a major titanium-bearing phase that would be expected to survive into the stratosphere of WASP-12b, where it could absorb at optical wavelengths, heat the atmosphere, and create a stratospheric thermal inversion (e.g., Hubeny et al. 2003; Fortney et al. 2006b, 2008a; Burrows et al. 2008; Spiegel et al. 2009) such as has been suggested for HD 209458b, HAT-P-7b, and several other transiting planets based on *Spitzer* observations (e.g., Burrows et al. 2007, 2008; Knutson et al. 2008, 2009a; Swain et al. 2009b; Madhusudhan & Seager 2009, 2010a; Spiegel & Burrows 2010; Christiansen et al. 2010).

However, Madhusudhan et al. (2011a) conclude that a strong stratospheric thermal inversion in the 0.01-1 bar region of WASP-12b can be statistically ruled out due to a poor fit to the secondary-eclipse *Spitzer*/IRAC data of Campo et al. (2011) and ground-based data of Croll et al. (2011). Instead, Madhusudhan et al. (2011a) suggest that the atmosphere of WASP-12b is enriched in carbon relative to solar elemental abundances, with WASP-12b spectra exhibiting strong absorption due to CO and CH₄, and much weaker absorption due to H₂O, as would be expected from an atmosphere with a C/O ratio greater than unity. In fact, the model-data comparisons of Madhusudhan et al. (2011a) suggest that a solar-like ratio of C/O = 0.54 for WASP-12b can be ruled out statistically at the 4.2 σ -significance level, whereas chemical-equilibrium models assuming C/O = 1 yield abundances of CO, H₂O, and CH₄ that are consistent with secondary-eclipse observations. Recently, Madhusudhan (2012) updated the WASP-12b secondary-eclipse analysis to include HCN and C₂H₂ in the spectral modeling, and their conclusions with respect to the high C/O ratio have not changed. Moreover, *HST* Wide Field Camera 3 (WF3) spectral observations by Swain et al. (2012) confirm the suggestion of a very low water abundance on WASP-12b, as well as a low TiO abundance, furthering the inference of a high C/O ratio for this planet. Swain et al. (2012) and Madhusudhan (2012) demonstrate that the WFC3 secondary-eclipse observations are well reproduced by high C/O ratio models. However, it is worth noting that Swain et al. (2012) favor a very-low-metallicity solution over a high-C/O-ratio solution in explaining the WFC3 observations because the high C/O ratio models provide a worse fit to the transit observations, especially at the short-wavelength end near 1.1-1.3 μ m. The degree to which Rayleigh scattering could be affecting the shorter wavelengths was not discussed.

In any case, the Madhusudhan et al. (2011a) analysis provided the first strong evidence for a high C/O ratio on a transiting exoplanet. Madhusudhan et al.

(2011b) further emphasized that TiO would not be abundant in giant-exoplanet atmospheres where C/O \geq 1, thus providing a theoretically consistent explanation for the lack of a stratospheric thermal inversion on WASP-12b. Kopparapu et al. (2012) followed up this analysis by developing photochemical models for WASP-12b for two different assumptions of the atmospheric C/O ratio; the molecules HCN and C₂H₂ were included in these models based on a suggestion by Moses & Visscher (2011) that these species would be important for high C/O ratios (see also Lodders 2010; Madhusudhan et al. 2011b). Kopparapu et al. (2012) found that C₂H₂ and HCN were even more abundant than CH₄ in their photochemical model with C/O = 1.08, and they suggested that C₂H₂ rather than CH₄ is responsible for the strong 8- μ m absorption on WASP-12b. We expand the Kopparapu et al. (2012) modeling by investigating the equilibrium and disequilibrium composition of WASP-12b for a variety of C/O ratios and by calculating the spectral consequences of abundant HCN and C₂H₂ for the carbon-rich cases.

3.3.1. WASP-12b Chemistry

Figure 10 illustrates how the thermochemical equilibrium composition of WASP-12b varies as a function of the atmospheric C/O ratio for our assumed nominal day-side thermal structure (see Fig. 1) and an assumed 3 \times solar metallicity. Because of WASP-12b's high temperatures, the chemical-equilibrium abundance of methane in the photosphere of WASP-12b is predicted to be smaller than that on the cooler HD 189733b or XO-1b, for similar assumptions of atmospheric metallicity and C/O ratio. Methane, with its relatively weak C-H bond, is less stable at high temperatures and low pressures than CO, which has a very strong carbon-oxygen bond. As with the other planets we have investigated, CO is again abundant for all assumptions of the C/O ratio, whereas H₂O and CO₂ are only important for C/O < 1, and HCN and C₂H₂ become more important for C/O > 1. At the high temperatures predicted for WASP-12b, HCN — which also has a strong carbon-nitrogen bond — quickly replaces CH₄ as the second-most abundant carbon-bearing molecule (behind CO) as the pressure decreases, even for C/O < 1. With increasing C/O ratio, C₂H₂ also becomes a major equilibrium constituent whose abundance can eventually exceed that of CO when C/O \gg 1. The implied large methane abundance required to fit the secondary-eclipse data in the Madhusudhan et al. (2011a) statistical analysis suggests a C/O ratio of \sim 2 or larger for WASP-12b (see Fig. 10); however, this conclusion changes when HCN and C₂H₂ opacities are included in the spectral models. For example, as is discussed in Section 3.3.2, at least part of the opacity hitherto attributed to CH₄ on WASP-12b could instead result from HCN and/or C₂H₂, which are abundant species in carbon-rich atmospheres with C/O ratios \geq 1 (see also Kopparapu et al. 2012; Madhusudhan 2012).

Disequilibrium processes like photochemistry and transport-induced quenching result in relatively minor changes in the profiles of the dominant species in our C/O = 1.015 model, except for HCN, C₂H₂, and atomic species (see Fig. 11). Hydrogen cyanide becomes a parent molecule of other photochemical products in much the same way as NH₃ and CH₄ do in cooler atmospheres.

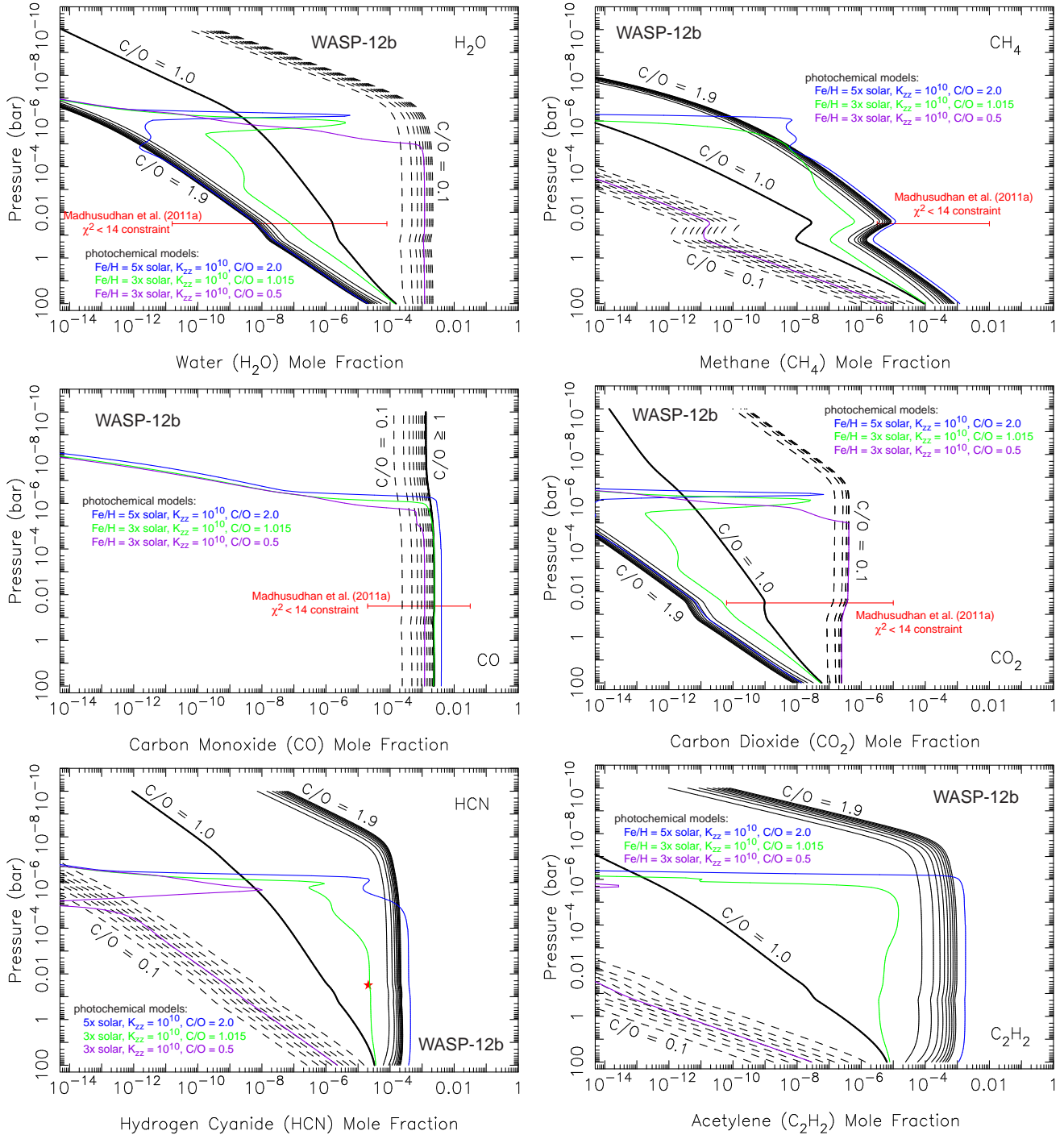


FIG. 10.— Mixing-ratio profiles for H_2O , CH_4 , CO , CO_2 , HCN , and C_2H_2 on WASP-12b from our thermochemical-equilibrium models with assumed $3\times$ solar metallicity but different assumed C/O ratios (ranging from 0.1 to 1.9, incrementing by 0.1 — dashed black lines for $C/O < 1$, solid lines for $C/O \geq 1$). The colored lines represent disequilibrium-chemistry results for models with $3\times$ solar metallicity and a solar-like C/O ratio of 0.5 (purple), a model with $3\times$ solar metallicity and a C/O ratio of 1.015 (green), and a model with $5\times$ solar metallicity and a C/O ratio of 2.0 (blue). All models have an assumed vigorous $K_{zz} = 10^{10} \text{ cm}^2 \text{ s}^{-1}$, which might be expected for such a highly irradiated planet. The red horizontal line segments represent abundance constraints from models presented in Madhusudhan et al. (2011a) based on the *Spitzer*/IRAC secondary-eclipse observations of Campo et al. (2011) and the ground-based *Ks*, *H*, and *K*-band secondary-eclipse observations of Croll et al. (2011). Note that HCN and C_2H_2 were not considered in the Madhusudhan et al. (2011a) analysis, and the red star in the HCN figure is from the present analysis and indicates the HCN abundance that best reproduces the secondary-eclipse data for our adopted nominal thermal structure shown in Fig. 1. A color version of this figure is presented in the online journal.

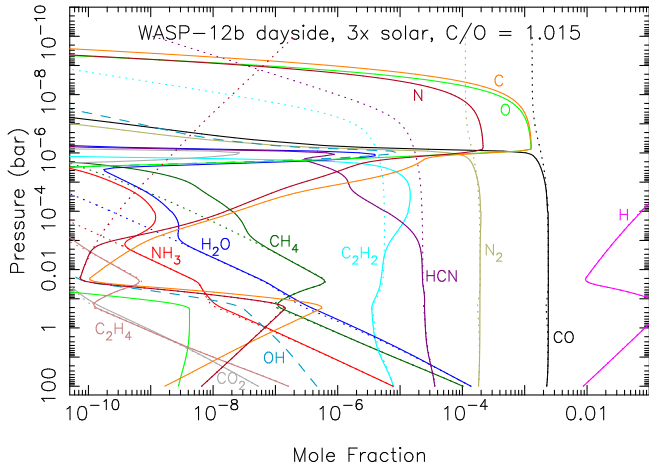
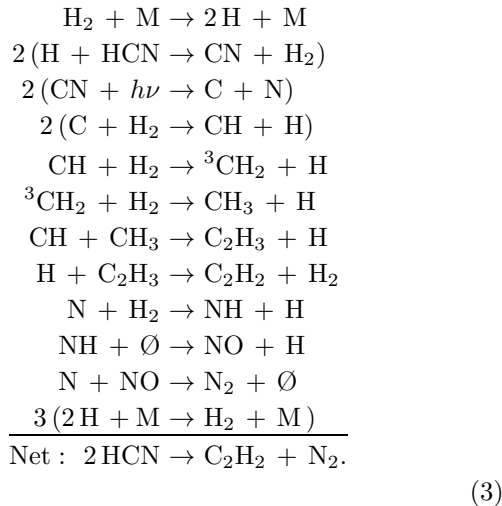


FIG. 11.— Mole-fraction profiles for several important species (as labeled) in a thermochemical and photochemical kinetics and transport model for WASP-12b. Model assumptions include $3\times$ solar metallicity, a C/O ratio of 1.015, and $K_{zz} = 10^{10} \text{ cm}^2 \text{ s}^{-1}$ (see also the green curves in Fig. 10). The dotted lines show the thermochemical-equilibrium abundances for the species, using the same color coding. Note that both HCN and C_2H_2 are more abundant than CH_4 throughout the middle atmosphere. A color version of this figure is available in the online journal.

Due to the high temperatures and large overall H abundance at high altitudes, kinetic loss of HCN via $\text{H} + \text{HCN} \rightarrow \text{CN} + \text{H}_2$ dominates over HCN photolysis as the main photochemical loss process. The CN radicals produced can recycle the HCN or become photolyzed themselves, leading to $\text{C} + \text{N}$. Atomic N can then react either with NO to form $\text{N}_2 + \text{O}$ or with CN to form $\text{N}_2 + \text{C}$, and the atomic carbon can react further to eventually produce C_2H_2 . The dominant C_2H_2 photochemical production scheme in our C/O = 1.015 model is



The acetylene abundance increases with altitude in the $\sim 2\text{-mbar}$ to $2\text{-}\mu\text{bar}$ region due to this HCN photochemistry, while the HCN abundance decreases. The nitrogen from HCN loss largely ends up as N_2 at pressures greater than $\sim 1 \mu\text{bar}$ and as atomic N at pressures less than $\sim 1 \mu\text{bar}$. In fact, no molecules (including H_2) survive at altitudes much above $\sim 1 \mu\text{bar}$, as the intense ultraviolet flux and large H abundance attack most molecular bonds and favor atomic species. Some photochemical production of H_2O , CH_4 , and NH_3 occurs from the CO and HCN pho-

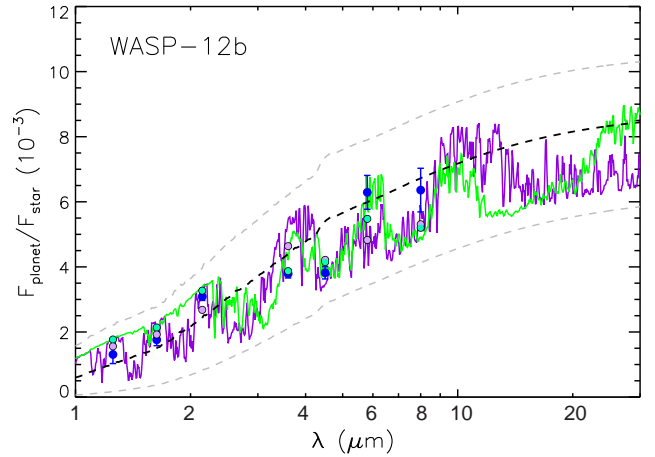


FIG. 12.— Secondary-eclipse spectra for WASP-12b. The solid lines represent synthetic spectra from the results of our disequilibrium chemistry models with $3\times$ solar metallicity, $K_{zz} = 10^{10} \text{ cm}^2 \text{ s}^{-1}$, and C/O ratios of either 1.015 (green) or 0.5 (purple). The blue circles with error bars represent the *Spitzer*/IRAC data from Campo et al. (2011) and ground-based data from Croll et al. (2011). The circles without error bars represent the model results for C/O = 1.015 (green) or 0.5 (purple) convolved over the *Spitzer* bandpasses. Note the better fit with the C/O = 1.015 model for this assumed metallicity and thermal structure, particularly at 2.1, 3.6, and $5.8 \mu\text{m}$. The dashed curves represent blackbodies with temperatures of 1800 K (bottom), 2500 K (middle), and 3000 K (top). A color version of this figure is available in the online journal.

tochemistry, but these species remain below ppm levels at pressures less than ~ 0.1 bar and only become significant at high pressures and in a narrow region centered near $\sim 1 \mu\text{bar}$ where photolysis of CO and N_2 is significant. In all, disequilibrium processes have less of an effect on hotter planets like WASP-12b than they do on cooler planets like HD 189733b and XO-1b (see also Liang et al. 2003, 2004; Zahnle et al. 2009b; Line et al. 2010, 2011a; Moses et al. 2011; Venot et al. 2012).

Our photochemical models for a high C/O ratio on WASP-12b differ somewhat from those of Kopparapu et al. (2012). Their upper atmosphere is cooler, which tends to reduce reaction rates. Transport-induced quenching of CH_4 and H_2O therefore become correspondingly more important, as expected, leading to increased abundances of H_2O and CH_4 . Their adopted temperature-pressure profile and C/O ratio of 1.08 also result in C_2H_2 being slightly more abundant than HCN in equilibrium throughout the photosphere, which can affect the photochemistry. However, the HCN and C_2H_2 vertical profiles of Kopparapu et al. (2012) are almost completely unaffected by photochemistry, in contrast to our models, for reasons that are unclear but likely have to do with different reaction mechanisms. Their main conclusion that HCN and C_2H_2 are important on WASP-12b for the case of $\text{C/O} \geq 1$ under both equilibrium and disequilibrium conditions is qualitatively supported by our models (see also Lodders 2010; Moses & Visscher 2011; Madhusudhan et al. 2011b; Madhusudhan 2012).

3.3.2. WASP-12b Spectra

Like methane, both HCN and C_2H_2 have bands that fall within the *Spitzer*/IRAC 8.0- μm spectral bandpass, and to a lesser extent within the short-wavelength end of the 3.6- μm spectral bandpass (e.g., Shabram et al. 2011). We find that all three molecules contribute to

the calculated flux in the 3.6 and 8- μm channels, but for our nominal thermal structure and C/O ratio ~ 1 , the channel-integrated flux at these wavelengths is particularly sensitive to the HCN mole fraction. For a $3\times$ solar metallicity and our adopted thermal structure, C/O ratios just over unity result in an HCN abundance that provides a good fit to the *Spitzer*/IRAC 3.6- μm band depth, while providing slightly too much absorption in the lower-signal-to-noise 8.0- μm band. This result will be model-dependent, particularly in terms of the relative contributions of different molecules for different thermal structures, but Fig. 12 demonstrates that our model with C/O = 1.015 provides a significantly better fit (with $\xi^2 < 2.6$) to the *Spitzer* data than the model with C/O = 0.5 (with $\xi^2 < 10.2$); this result is consistent with the detailed statistical analysis of Madhusudhan et al. (2011a). The C/O = 1.015 model has much less absorption at 5.8 μm and much more absorption at 3.6 μm than the C/O = 0.5 model, and the predicted relative strengths in all four *Spitzer*/IRAC bands are much more consistent with observations for the higher C/O ratio model. We therefore concur with the suggestion of Madhusudhan et al. (2011a) that WASP-12b could be a carbon-enriched planet, although in our model it is HCN rather than CH_4 that provides the dominant opacity source in the 3.6 and 8.0 μm channels (see also Section 4 and Madhusudhan 2012). Note that a high C/O ratio model for WASP-12b is also more consistent with the recent *HST* WFC3 secondary-eclipse observations of Swain et al. (2012) in which a very low water abundance is needed to explain the nearly featureless 1.0-1.7 micron spectrum of WASP-12b (e.g., Swain et al. 2012; Madhusudhan 2012).

The large predicted HCN abundance on a putative carbon-rich WASP-12b is also likely to affect its near-infrared transit spectrum, where Cowan et al. (2012) observe a larger transit depth in the 3.6- μm *Spitzer* channel than in the 4.5 μm channel. Cowan et al. (2012) did not consider the possible influence of HCN on the 3.6- μm absorption, and in fact only considered enhanced CO abundances as a consequence of a potential carbon-rich scenario. Future transit simulations should consider the influence of HCN and C_2H_2 . At 1-2 μm , the spectrum in the high C/O ratio case is much more featureless than the solar C/O ratio case, where water absorption bands are prominent.

3.4. CoRoT-2b Results

The transiting planet CoRoT-2b, discovered by Alonso et al. (2008), has often been called a “misfit” because of its unusually large radius (e.g., Alonso et al. 2008; Gillon et al. 2010; Guillot & Havel 2011) and because traditional models that assume solar elemental abundances cannot explain its unusual flux ratios from secondary-eclipse observations in the *Spitzer*/IRAC channels at 3.6, 4.5, and 8.0 μm , regardless of whether the planet is assumed to have a stratospheric thermal inversion or not (Gillon et al. 2010; Deming et al. 2011). The main problem is an anomalously low flux at 8.0 μm and an unusually large 4.5- μm /8.0- μm flux ratio. Madhusudhan (2012) suggests that all the secondary-eclipse observations for CoRoT-2b can be reproduced to within their $1-\sigma$ uncertainties for chemically plausible models with C/O ≥ 1 ; Madhusudhan (2012) also finds

good solutions for oxygen-rich models, but those models tend to have implausibly large CH_4/CO abundance ratios. Because there is no *Spitzer*/IRAC data available for CoRoT-2b from the 5.8- μm IRAC channel, model solutions for CoRoT-2b will tend to be more degenerate, but if Madhusudhan (2012) is correct in his suggestion of a carbon-rich atmosphere, then CoRoT-2b would fall within the C2 regime in their classification scheme.

3.4.1. CoRoT-2b Chemistry

Figure 13 illustrates how the thermochemical-equilibrium composition of CoRoT-2b varies as a function of the atmospheric C/O ratio for our assumed nominal dayside thermal structure (see Fig. 1) and an assumed $0.5\times$ solar metallicity. The low metallicity we are considering here is required to prevent too much absorption from CO in the *Spitzer*/IRAC channel at 4.5 μm for our assumed thermal structure; a warmer atmosphere would allow higher metallicities while still being consistent with the data. As with all the other planets we have considered, CO is abundant in chemical equilibrium for all assumptions of the C/O ratio, whereas H_2O and CO_2 are only abundant for C/O < 1 , and CH_4 , HCN, and C_2H_2 become more abundant for C/O > 1 . For a model with a thermal structure similar to our adopted nominal profile shown in Fig. 1, Madhusudhan (2012) finds good fits to the Alonso et al. (2010), Gillon et al. (2010), and Deming et al. (2011) secondary-eclipse data for the species mole fractions marked by a star in Fig. 13. These constraints imply that CO and CH_4 are abundant, whereas H_2O and CO_2 remain below ppm levels. It appears that a C/O ratio near 1.1 can readily satisfy all the these constraints. The relatively low upper atmospheric temperatures adopted for our nominal model suggest that photochemistry will be important on CoRoT-2b, as we found for XO-1b and HD 189733b.

Indeed, Fig. 14 shows that disequilibrium chemistry is important for our CoRoT-2b model with an assumed C/O ratio of 1.1, a subsolar metallicity of $0.5\times$ solar, and $K_{zz} = 10^9 \text{ cm}^2 \text{ s}^{-1}$. Transport-induced quenching of water is very important, enhancing the H_2O atmospheric column abundance by about an order of magnitude, and CO photochemistry further enhances the H_2O abundance in the upper atmosphere by many orders of magnitude. Photochemical production of water occurs via CO photolysis in the upper stratosphere to produce C + O, followed by reactions of O with H_2 to form OH, which reacts with H_2 to form water. The atomic C can react with NO to form CN and eventually HCN (see scheme (2) above) or the C can react with H_2 to form CH, which eventually goes on to produce C_2H_2 . We are even seeing a non-trivial formation rate of small C_3H_x compounds at high altitudes in the model from reaction of C and/or CH with C_2H_2 ; these C_3H_x species could be soot precursors, although benzene and complex nitriles themselves never exceed ppb levels in this constantly-illuminated model. Transport-induced quenching also affects CH_4 , HCN, NH_3 , CO_2 , and many other species in the middle atmosphere, whereas photochemistry affects profiles in the upper atmosphere. Although photochemical production of CO_2 greatly enhances its abundance in the upper atmosphere, the column abundance in the photosphere is still quite small, and CO_2 should have little influence on spectra. The chemistry of a carbon-rich

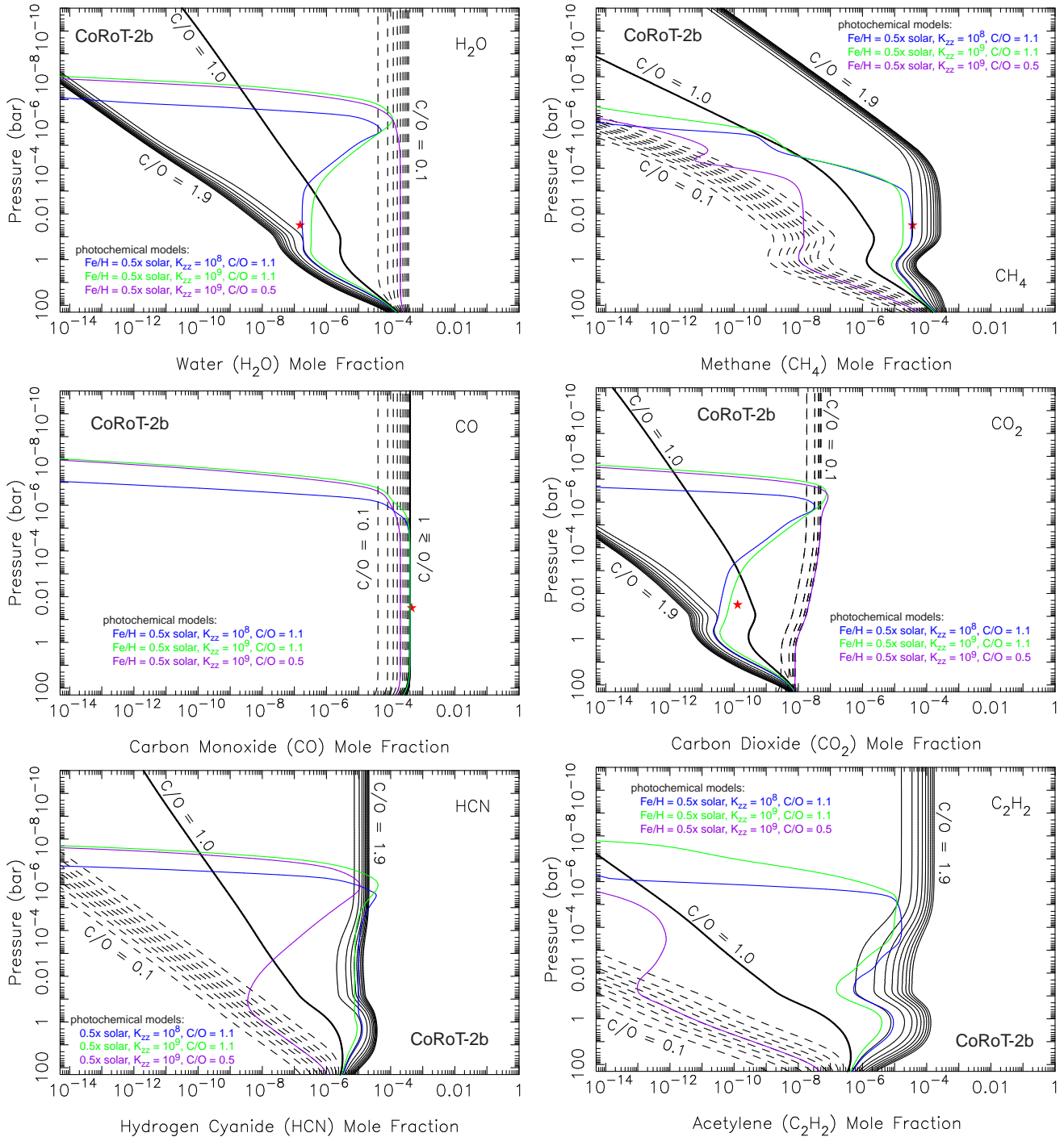


FIG. 13.— Mixing-ratio profiles for H_2O , CH_4 , CO , CO_2 , HCN , and C_2H_2 on CoRoT-2b from our thermochemical-equilibrium models with assumed $0.5\times$ solar metallicity but different assumed C/O ratios (ranging from 0.1 to 1.9, incrementing by 0.1 — dashed black lines for $\text{C/O} < 1$, solid lines for $\text{C/O} \geq 1$). The colored lines represent disequilibrium-chemistry results for models with a solar-like C/O ratio of 0.5 and $K_{zz} = 10^9 \text{ cm}^2 \text{ s}^{-1}$ (purple), a model with a C/O ratio of 1.1 and $K_{zz} = 10^9 \text{ cm}^2 \text{ s}^{-1}$ (green), and a model with a C/O ratio of 1.1 and $K_{zz} = 10^8 \text{ cm}^2 \text{ s}^{-1}$ (blue). All models have an assumed atmospheric metallicity of $0.5\times$ solar. The red stars represent abundance constraints from a preliminary model (Madhusudhan 2012) based on the *Spitzer*/IRAC secondary-eclipse observations of Gillon et al. (2010) and Deming et al. (2011) and the ground-based secondary-eclipse *Ks*-band observations of Alonso et al. (2010), in which HCN and C_2H_2 were not considered in the analysis. A color version of this figure is presented in the online journal.

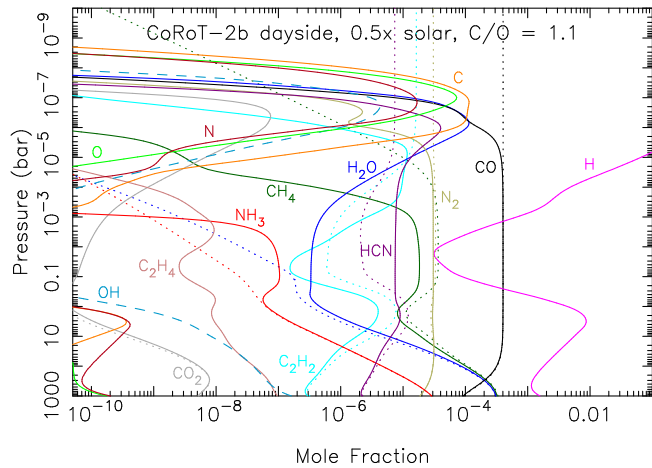


FIG. 14.— Mole-fraction profiles for several important species (as labeled) in a thermochemical and photochemical kinetics and transport model for CoRoT-2b. Model assumptions include $0.5\times$ solar metallicity, a C/O ratio of 1.1, and $K_{zz} = 10^9 \text{ cm}^2 \text{ s}^{-1}$ (see also the green curves in Fig. 13). The dotted lines show the thermochemical-equilibrium abundances for some of the species, using the same color coding. Note the enhanced disequilibrium abundances of HCN, H_2O , NH_3 , and CO_2 over equilibrium values. A color version of this figure is available in the online journal.

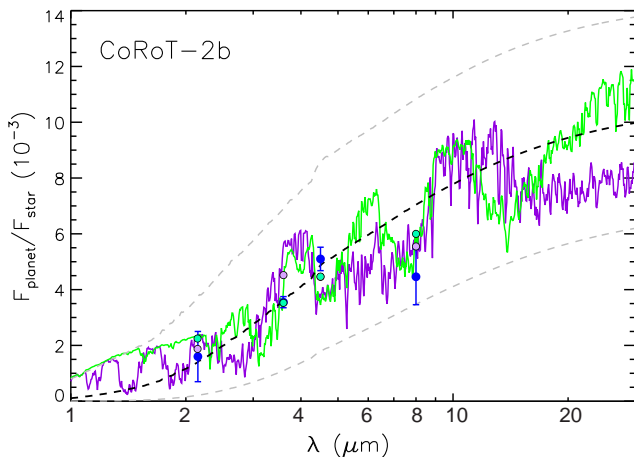


FIG. 15.— Secondary-eclipse spectra for CoRoT-2b. The solid lines represent synthetic spectra from the results of our disequilibrium chemistry models with $0.5\times$ solar metallicity, $K_{zz} = 10^9 \text{ cm}^2 \text{ s}^{-1}$, and C/O ratios of either 1.1 (green) or 0.5 (purple). The blue circles with error bars represent the *Spitzer*/IRAC data from Gillon et al. (2010) and Deming et al. (2011) and ground-based data from Alonso et al. (2010). The circles without error bars represent the model results for C/O = 1.1 (green) or 0.5 (purple) convolved over the spectral bandpasses. Note the better fit with the C/O = 1.1 model at $3.6 \mu\text{m}$ for this particular assumed metallicity and thermal structure. A color version of this figure is available in the online journal.

CoRoT-2b is similar to that of HD 189733b and XO-1b, which is covered in more detail in Sections 3.1.1 & 3.2.1; the chemistry of a solar-like-composition CoRoT-2b is similar to that of other “warm” transiting planets (see Moses et al. 2011 and Line et al. 2010 for further details).

3.4.2. CoRoT-2b Spectra

Figure 15 shows how two models with different C/O ratios compare with the *Spitzer*/IRAC data of Gillon et al. (2010) and Deming et al. (2011) and the ground-based data of Alonso et al. (2010) at secondary eclipse. Both

models exhibit too much absorption at $4.5 \mu\text{m}$, which demonstrates why we did not investigate models with higher metallicities for this particular thermal structure. Both models exhibit less flux in the $8\text{-}\mu\text{m}$ channel than in the $4.5 \mu\text{m}$ channel, in contrast to observations, which further emphasizes the unusual observed $4.5\text{-}\mu\text{m}/8\text{-}\mu\text{m}$ flux ratio for this planet (see Deming et al. 2011; Madhusudhan 2012), although both models are within $\sim 1.5\text{-}\sigma$ of the uncertainties at these wavelengths. The main difference between the models lies in the $3.6\text{-}\mu\text{m}/4.5\text{-}\mu\text{m}$ flux ratio and in the overall fit in the $3.6\text{-}\mu\text{m}$ channel, for which the C/O = 1.1 model provides a significantly better fit to the existing secondary-eclipse data. In all, this carbon-rich model provides a statistically better fit ($\xi^2 = 1.3$) than the solar-composition models presented here ($\xi^2 = 7.2$) and in Madhusudhan (2012) and Deming et al. (2011), while still having theoretically consistent species abundances. The suggestion of Madhusudhan (2012) that CoRoT-2b could have a carbon-rich atmosphere is therefore viable, although further observations at additional wavelengths would be required to fully test the suggestion.

As an aside, we note that unlike the case for the very hot WASP-12b or the much cooler XO-1b, our nominal thermal profile for CoRoT-2b first crosses the enstatite and forsterite condensation curves right within the planet’s photosphere (for solar-like elemental compositions), which suggests that silicate clouds could have more spectral consequences on CoRoT-2b than they do on much hotter or cooler planets. Opacity from thick clouds can reduce the depth (and broadness) of absorption bands and make the observed planetary spectrum appear more like a blackbody. We note, however, that the observed secondary-eclipse data for CoRoT-2b do not much resemble a blackbody, particularly in terms of the deep absorption in the $8\text{-}\mu\text{m}$ channel. If clouds were present near ~ 0.1 bar or deeper, they would have relatively little effect on the photochemistry of C, N, and O-bearing species. High-altitude clouds located at 10^{-3} mbar or above, on the other hand, could shield species from photolysis, with some interesting consequences. We also note that the host star for CoRoT-2b is very young and spectrally active (Bouchy et al. 2008; Guillot & Havel 2011), which would result in a high x-ray and EUV flux and enhanced charged particle fluxes that would be conducive for ion chemistry in the atmosphere of CoRoT-2b. As mentioned by Moses et al. (2011), Titan-like ion chemistry at high altitudes could enhance the destruction of N_2 (and perhaps CO) and enhance the production of complex hydrocarbons, which could further influence spectral behavior.

4. IMPLICATIONS WITH RESPECT TO SPECTRA

The atmospheric composition of carbon-rich planets differs considerably from that of solar-composition planets, and those differences have spectral implications, as is obvious from Figs. 4, 6, 9, 12, and 15. Photochemical production of HCN and C_2H_2 is efficient enough on cooler exoplanets (even those that are only mildly carbon-enhanced) that these species could affect spectra in certain wavelength regions. Acetylene would provide opacity mainly in the $13\text{-}15 \mu\text{m}$ region, and to a lesser extent in the ~ 3 and $7\text{-}8 \mu\text{m}$ regions (with the latter bands falling within the *Spitzer* 3.6 and $8.0\text{-}\mu\text{m}$ channels). Hy-

drogen cyanide would provide opacity mainly in the $\sim 3\text{-}\mu\text{m}$, $6.5\text{-}7.8\ \mu\text{m}$, and $12\text{-}16\ \mu\text{m}$ regions (with broader wavelength ranges for higher temperatures). Even on the hottest transiting exoplanets, species like HCN can have a major influence on the total atmospheric opacity if the atmospheric C/O ratio exceeds unity. For example, Fig. 16 shows the major influence that HCN has on the infrared spectra of our nominal carbon-rich WASP-12b model with C/O = 1.015. Although C_2H_2 has relatively little influence on the spectrum, only becoming noticeable in the $\sim 3\text{-}\mu\text{m}$ region, HCN opacity completely dominates in several wavelength regions, even surpassing the contribution of CH_4 , CO, H_2O , and other molecules at $\sim 2.4\text{-}4.1\ \mu\text{m}$ and in the $6\text{-}10\ \mu\text{m}$ region. Note that CH_4 opacities at high temperatures are poorly known and may be underestimated by as much as two orders of magnitude or more in our spectral calculations. If we approximate this effect by increasing the CH_4 abundance by a factor of 100, we see that CH_4 opacity could still be important on WASP-12b, but that does not change the fact that HCN is likely a major opacity source in the *Spitzer* 3.6 and $8.0\ \mu\text{m}$ channels. Clearly, HCN is a potentially important molecule that can contribute to exoplanet spectral behavior and should be included in analyses of exoplanet spectra; C_2H_2 and NH_3 are important disequilibrium species under some conditions and should also be considered if those conditions are met (e.g., potentially high C/O ratio or cooler atmosphere; see also Moses et al. 2011, Kopparapu et al. 2012).

Note, however, that to truly determine relative molecular abundances from exoplanet spectra, more detailed information on the line parameters (including intensities) from hot bands is needed in the molecular spectroscopy databases like GEISA and HITRAN (Jacquinet-Husson et al. 2008; Rothman et al. 2009). There is currently insufficient published high-temperature information on CH_4 , HCN, and C_2H_2 to reliably evaluate their potential quantitative contributions to the spectra.

Carbon dioxide can influence the spectra, particularly near $\sim 2\ \mu\text{m}$, $\sim 4.3\ \mu\text{m}$, and in the $14\text{-}16\ \mu\text{m}$ region. Our carbon-enhanced nominal disequilibrium models that provide good fits to the *Spitzer*/IRAC data tend to have CO_2 abundances lower than those derived from the analyses of Madhusudhan & Seager (2009), Madhusudhan et al. (2011a), and Madhusudhan (2012) for these four exoplanets (see Figs. 2, 7, 10, & 13). Of all the *Spitzer*/IRAC channels, carbon dioxide has the most influence on the flux in the $4.5\text{-}\mu\text{m}$ channel, and Figs. 4, 6, 9, & 12 demonstrate that our band-integrated fluxes at $4.5\ \mu\text{m}$ do indeed fall slightly above the IRAC-derived fluxes at this wavelength for HD 189733b, XO-1b, and WASP-12b (CoRoT-2b being the exception). Because other molecules such as CO contribute to the flux in this IRAC channel, an improved fit would be obtained for slight increases in the assumed metallicity of these planets; therefore, our low derived CO_2 abundances do not seem to be a major problem for the *Spitzer* IRAC fits.

That is not the case at near-IR wavelengths, however, at least for HD 189733b. Note from Figs. 2, 7, 10, & 13 that our predicted CO_2 mole fraction for all four of the exoplanets investigated never exceeds ppm levels, regardless of the C/O ratio, for both equilibrium and disequilibrium chemistry. Even for $10\times$ solar metallicities, Fig. 17

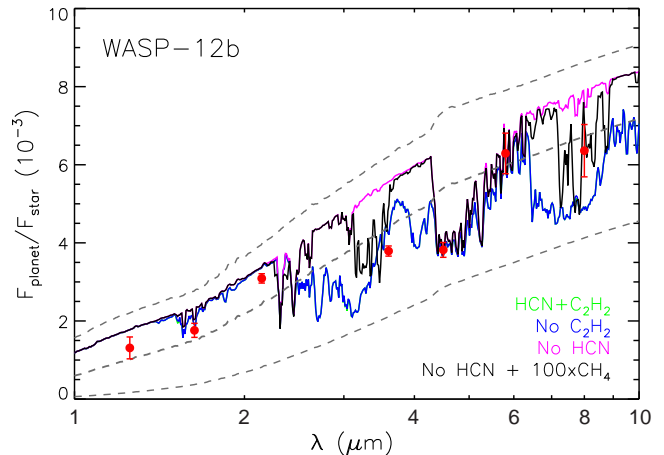


FIG. 16.— The contribution of various molecules in our $3\times$ solar metallicity, C/O = 1.015 disequilibrium-chemistry model to the predicted secondary-eclipse spectra for WASP-12b. The green curve represents synthetic spectra from our nominal model (see Figs. 11 & 12), whereas the blue curve is the same model with C_2H_2 eliminated. The two curves overlap almost exactly, illustrating the relative insignificance of C_2H_2 as an opacity source in this model. For the magenta curve, the contribution of HCN has been eliminated from the nominal model; a comparison of the magenta curve with the blue and/or green curves illustrates the dominance of HCN opacity in controlling the spectra behavior in many wavelength regions in our model. The black curve is a synthetic spectrum without the contribution of HCN, but in which the CH_4 abundance has been increased by a factor of 100. The red circles with error bars represent the *Spitzer* and ground-based secondary-eclipse data of Campo et al. (2011) and Croll et al. (2011). The dashed lines are blackbody curves for assumed temperatures of 1800 K (bottom), 2500 K (middle), and 3000 K (top). A color version of this figure is available in the online journal.

demonstrates that carbon dioxide is not expected to be a major product on hot Jupiters, and photochemistry does not change this conclusion.

The relative unimportance of CO_2 in our chemical models is in stark contrast to the conclusions based on secondary-eclipse observations of HD 189733b in the near-infrared obtained with HST/NICMOS (Swain et al. 2009a). The constraints for CO_2 based on this dataset range from a derived mole fraction of $10^{-6}\text{-}10^{-1}$ (Swain et al. 2009a), to a best fit of $\sim 7\times 10^{-4}$ (Madhusudhan & Seager 2009), to a best fit of $\sim 2\times 10^{-3}$ (Lee et al. 2012), to derived values of $(1.7\text{-}6.7)\times 10^{-3}$ (Line et al. 2011b). Such large CO_2 abundances are inconsistent with the *Spitzer*/IRAC data in the $4.5\text{-}\mu\text{m}$ channel, which has led to the suggestion of atmospheric variability (Madhusudhan & Seager 2009). However, note that the retrievals from this data set suggest $\text{CO}_2/\text{H}_2\text{O}$ ratios of ~ 3 (Lee et al. 2012) or even ~ 30 (Line et al. 2011b), which is not likely for a hydrogen-dominated planet. In fact, to get CO_2 abundances comparable to those of H_2O under thermochemical-equilibrium conditions for our nominal thermal structure, HD 189733b would have to have a metallicity of order ~ 2000 , at which point H_2 would no longer be the dominant constituent by number — a suggestion seemingly inconsistent with the planet’s overall density and mass-radius relationship (Marley et al. 2007).

Disequilibrium chemistry cannot help resolve this problem. The dominant production mechanism for CO_2 is $\text{CO} + \text{OH} \rightarrow \text{CO}_2 + \text{H}$, which is indeed effective on the dayside of HD 189733b due to OH production from

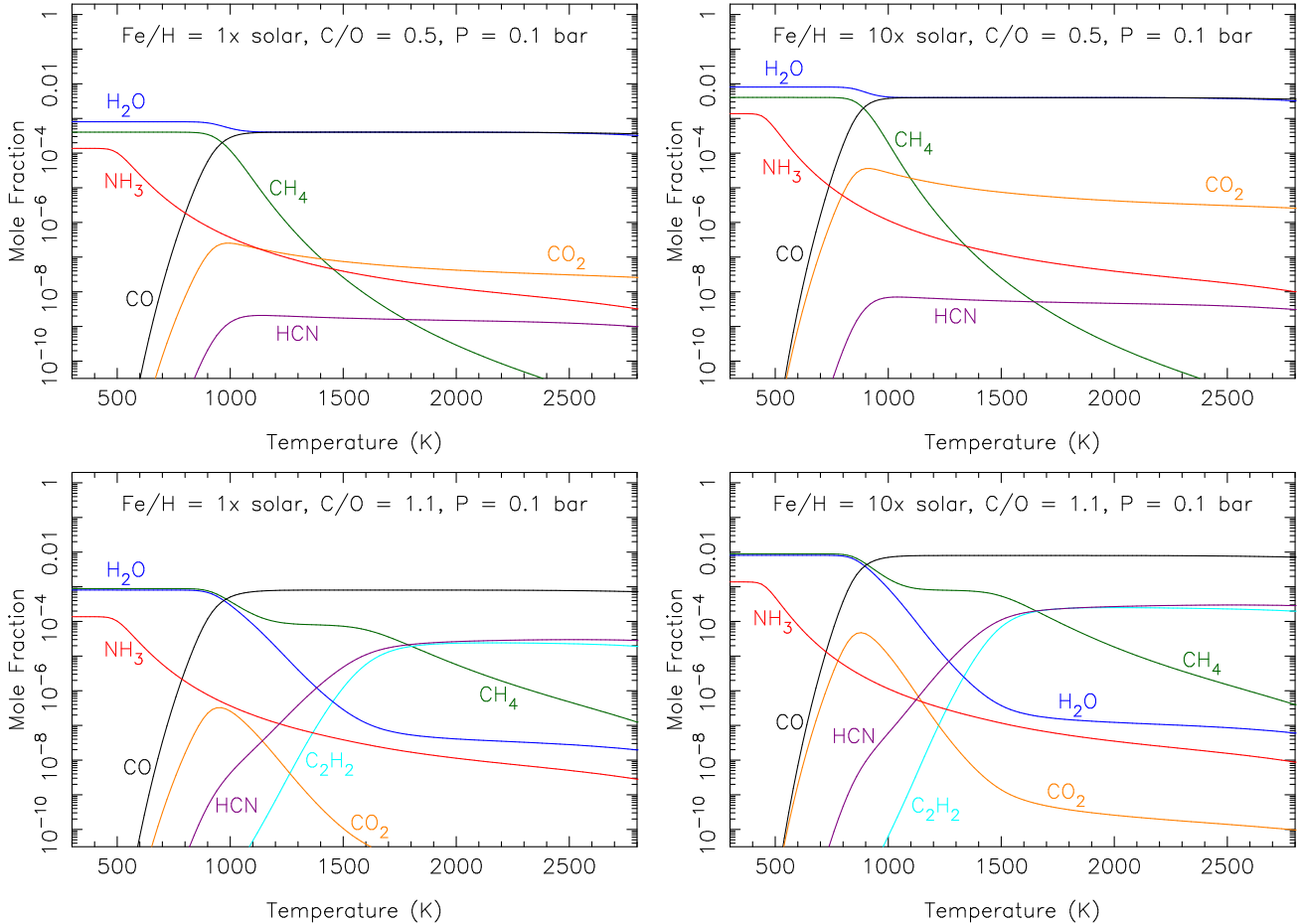


FIG. 17.— The variation in the thermochemical-equilibrium abundances of key spectrally active species as a function of temperature at 0.1 bar, which is a typical pressure predicted to be within the infrared photospheres of hot Jupiters, for $1\times$ solar metallicity and $C/O = 0.5$ (top left), for $10\times$ solar metallicity and $C/O = 0.5$ (top right), for $1\times$ solar metallicity and $C/O = 1.1$ (bottom left), and for $10\times$ solar metallicity and $C/O = 1.1$ (bottom right). Note the relatively low CO_2 abundance in relation to H_2O for all temperatures, even for the more favorable case of $10\times$ solar metallicity at a C/O ratio of 0.5. A color version of this figure is available in the online journal.

H_2O photolysis (and other kinetic processes) and due to the large overall abundance of CO . The main problem is that the reverse of this reaction is also effective at atmospheric conditions on HD 189733b, due to the large available H abundance and the relatively high atmospheric temperatures. The forward and reverse reaction rates balance each other to a large degree, and although there is a small positive net production of CO_2 in our dayside atmospheric models, the CO_2 column abundance never achieves the levels needed to explain the HST/NICMOS secondary-eclipse observations of Swain et al. (2009a). It is possible that we are missing some key photochemical mechanism that effectively converts water to CO_2 on transiting exoplanets, which would be needed to explain a high derived CO_2/H_2O ratio (see Lee et al. 2012; Line et al. 2011b), but given the efficiency of H_2O recycling in a hydrogen-dominated atmosphere (see also Moses et al. 2011; Line et al. 2010), it is hard to imagine that any chemical mechanism could produce this result while hydrogen is still the dominant atmospheric constituent.

The problem could potentially be resolved if the absorption attributed to CO_2 in the Swain et al. (2009a) NICMOS data actually resulted from some other atmospheric constituent. Species like NH_3 , HCN , and C_2H_2

come readily to mind as candidates, as they are all relatively abundant in our disequilibrium models, particularly for super-solar C/O ratios (for the case of HCN and C_2H_2) or rapid atmospheric mixing at depth (for the case of NH_3). Hydrogen cyanide has strong bands in the $\sim 3\text{-}\mu\text{m}$ region and much weaker bands in the $\sim 1.85\text{ }\mu\text{m}$ and $\sim 1.53\text{ }\mu\text{m}$ regions; as such, HCN seems unlikely to cause significant absorption in the needed $1.9\text{-}2.2\text{ }\mu\text{m}$ range, despite the relatively large predicted column abundance of $\sim 1\times 10^{19}\text{ cm}^{-2}$ above 1 bar in our nominal $C/O = 0.88$ disequilibrium model. For the same model, NH_3 and C_2H_2 have column abundances of $\sim 2.5\times 10^{19}$ and $\sim 2.5\times 10^{16}\text{ cm}^{-2}$, respectively. Acetylene (and HCN) could be more abundant than we derive if the upper atmosphere is cooler than we have assumed (e.g., Moses et al. 2011) or if ion chemistry enhances its abundance, but the C_2H_2 bands near ~ 1.53 and $\sim 2.45\text{ }\mu\text{m}$ do not seem good spectral matches to the NICMOS data. Ammonia has bands centered near ~ 1.97 and $2.2\text{-}2.4\text{ }\mu\text{m}$ that could be of interest to the NICMOS data, particularly given that models with different assumed thermal structures and K_{zz} values (Moses et al. 2011) predict a significantly larger NH_3 abundance than the models shown here. Although the NH_3 band at $1.97\text{ }\mu\text{m}$ lines up well with the minimum in flux seen in the

NICMOS spectra, the continued absorption in the ~ 2.1 μm region seen in the NICMOS data does not seem consistent with NH_3 ; however, due to the likely presence of NH_3 on HD 189733b and other transiting planets, further investigation is warranted. At the very least, NH_3 and HCN should be considered in both near-IR and thermal-IR spectral models for hot Jupiters, as these molecules are important disequilibrium products for a variety of C/O ratios, as well as important equilibrium products for cooler planets and/or for planets with high C/O ratios.

Models that contain more ammonia (e.g., because of stronger atmospheric mixing or a cooler thermal structure at depth) could also help improve the discrepancy between our best-fit solutions to the secondary-eclipse *Spitzer* IRAC data as compared with the IRS spectra for HD 189733b (see also Madhusudhan & Seager 2009). A hot lower atmosphere was found necessary to fit the high flux in the 3.6 μm -channel IRAC data in both our analysis and that of Madhusudhan & Seager (2009), but that solution also caused excess flux in the 9–12 μm region that is inconsistent with the IRS data (see Fig. 4). Moses et al. (2011) demonstrate that the flux in the spectral models at ~ 9 –12 μm is considerably reduced when opacity from a moderate amount of quenched NH_3 is included in the calculations (see Fig. 13 of Moses et al. 2011). However, the very recent *Spitzer* IRAC analysis of Knutson et al. (2012) suggests a very large 7.5σ reduction in the 3.6- μm flux at secondary eclipse, eliminating the need for such a warm lower atmosphere to explain the 3.6- μm data and reducing the model flux in the 9–12 μm region to be more in line with the IRS observations (see Section 3.1.3 and Fig. 6 for more details).

Although we have focused on secondary-eclipse observations in this paper, transit observations can also provide compositional information. The C/O ratio is a bulk atmospheric property that does not change on observational time scales. Atmospheric temperatures, on the other hand, change relative quickly through much of the photospheric region due to changes in the incidence angle of the radiation coming from the host star and to the relatively short radiative heating and cooling time scales (e.g., Barman et al. 2005). Dynamical time scales are of order $\sim 10^5$ s, which is typically longer than radiative time scales, allowing horizontal thermal gradients to be maintained (e.g., Showman et al. 2009). The average temperature structure therefore changes with viewing geometry (e.g., Knutson et al. 2007). If chemical time scales are shorter than dynamical time scales, the composition will also change with viewing geometry.

Chemical time scales range from very short ($\ll 10^5$ s) in the deepest, hottest regions below the photosphere and in the uppermost regions of the photosphere where disequilibrium photochemistry is active, to $> 10^5$ s in the mid-to-lower photosphere. In the mid-to-upper photosphere, chemical time scales can either be $\lesssim 10^5$ s or $\gtrsim 10^5$ s, depending on stratospheric temperatures. When chemical lifetimes are longer than transport time scales, which is likely true for a good portion of the photosphere on the cooler transiting exoplanets, then transport-induced quenching can operate effectively to homogenize composition horizontally as well as vertically (e.g., Cooper & Showman 2006), significantly reducing

the temperature-related equilibrium compositional variations shown in plots like Fig. 17. However, chemical lifetimes will be shorter on warmer planets and for certain altitude regions on cooler planets, making compositional variations possible between transit observations (which are sensitive to the limb atmosphere at the terminators) and eclipse observations (which are sensitive to the fully illuminated dayside atmosphere). Accurate predictions of the composition as a function of planetary viewing angle will therefore require more sophisticated time-variable disequilibrium models, which we delegate to future investigations.

5. THE CASE FOR PLANETARY C/O RATIOS GREATER THAN THE HOST STAR

According to our current understanding of star formation, the elemental ratios within a stellar photosphere reflect to a large degree the elemental ratios of the protostellar nebula in which the star formed, except for a slight depletion in heavy elements relative hydrogen due to later diffusive settling in the stellar atmosphere (e.g., Lodders et al. 2009, and references therein). Since planets also formed within that same nebula (i.e., protoplanetary disk), one might naively expect giant planets that efficiently accrete nebular gas to have elemental ratios that match that of the host star and bulk protoplanetary disk. In that naive view, giant planets with high C/O ratios would then be expected to derive from a protoplanetary disk with high bulk C/O ratios, and their host stars should be similarly carbon-enriched. Many factors can complicate this naive picture (see below), but detailed evolution models for WASP-12b suggest that a protoplanetary disk with a supersolar C/O ratio is required to produce WASP-12b with $\text{C/O} \geq 1$ (Madhusudhan et al. 2011b).

Although most stars appear to have near-solar relative abundances of carbon and oxygen, there is some observational evidence for a C/O-rich tail of the stellar population distribution, indicating a non-trivial percentage of stars with C/O ratios greater than 1 (Ecuivillon et al. 2004, 2006, Delgado Mena et al. 2010, Petigura & Marcy 2011; see also Bond et al. 2010). Gaidos (2000) points out the C/O ratio of the gas in the galactic disk is likely increasing with time, leading to a C/O ratio that is larger for younger planetary systems in our galaxy and for those farther away from the galactic bulge, and Petigura & Marcy (2011) provide observational evidence that stars with planetary systems have statistically higher C/O ratios than those without planets. Both these factors could potentially explain observations of carbon-rich giant planets. On the other hand, Fortney (2012) notes that stars with C/O ratios greater than 1 have likely been overestimated in observational studies (Ecuivillon et al. 2004, 2006; Delgado Mena et al. 2010; Petigura & Marcy 2011) such that carbon-rich stars (and by correlation, carbon-rich protoplanetary disks) are more likely to be very rare in the galaxy. In this vein, it is notable that the host star WASP-12 appears to have a subsolar C/O ratio of $0.40^{+0.11}_{-0.07}$ (Petigura & Marcy 2011), in contrast to the suggestion of Madhusudhan et al. (2011a) and the work presented here that WASP-12b’s atmosphere could be carbon rich, and in conflict with the naive view of similar elemental ratios in a giant planet and its host

star. How then could a giant planet develop a C/O ratio different from its host star?

Several processes — some better understood than others — can conspire to produce this result. Disk chemistry is not uniform with location and time, and physical and chemical fractionations can lead to different C/O ratios in the nebular gas and/or solids (e.g., Krot et al. 2000; Cuzzi et al. 2005; Petaev et al. 2005; Lodders 2010). Evidence from meteorites in our own solar system suggests that although the bulk nebula had a solar C/O ratio, there were pockets that must have been both oxygen-rich and oxygen-poor (at different locations and/or times) to account for certain mineral assemblages in different meteorite classes, with enstatite chondrites in particular suggesting some regions in the solar nebula had $C \approx O$ at the time and location in which the enstatite chondrites were formed (cf. Larimer 1975; Krot et al. 2000; Hutson & Ruzicka 2000; Pasek et al. 2005).

One obvious fractionation process is condensation. Condensation of water ice at the “snow line” in a diffusive or turbulently mixed nebula progressively depletes water vapor from the inner nebula (Stevenson & Lunine 1988), and this process plus inward drift of ice grains from the outer nebula (Stepinski & Valageas 1997) leads to a pile up of water-ice solids near the snow line that can greatly facilitate the formation of giant planets (assuming the core-accretion model for giant-planet formation; e.g., Mizuno et al. 1978; Pollack et al. 1996). As more water becomes trapped in proto-giant-planet cores and other planetesimals, the overall C/O ratio of the remaining vapor increases, and water-vapor transport to this cold trap can eventually leave the inner nebula depleted in water (Stevenson & Lunine 1988; Cyr et al. 1998), although there may be temporary regions of enhanced water vapor where inwardly drifting icy grains evaporate (Cuzzi & Zahnle 2004; Ciesla & Cuzzi 2006). The outer nebula will also be depleted in water vapor wherever water ice condenses. Several such condensation/evaporation fronts for different ices occur at various radial distances in the nebula, leading to solids with different degrees of carbon and oxygen enrichments/depletions and vapor with complementary elemental depletions/enrichments, all of which can influence the composition of giant-planet atmospheres (Lodders 2004; Dodson-Robinson et al. 2009; Öberg et al. 2011). Solids of sufficient size can decouple from the gas and evolve differently in the disk such that although the solar nebula had a bulk solar C/O ratio initially, the relative abundances of carbon and oxygen in the solids and gas varies with location and evolves with time (e.g., Ciesla & Cuzzi 2006). The C/O ratio in the atmosphere of a giant planet then depends on the location and timing of its formation and the subsequent evolutionary history.

If one assumes that a planet’s carbon enrichment is largely due to the accretion of solid material, which could incidentally also result in planetary metallicities enhanced over the host star’s, then there is a limited region within a protoplanetary disk from which the planet could have accreted these carbon-enriched solids (e.g., Lodders 2004, 2010). Water ice condenses beyond the H₂O snow line (which forms initially near ~ 5 AU in the solar nebula but moves inward with time; see Ciesla & Cuzzi 2006), whereas carbon can remain pre-

dominantly as gas-phase CO out to its condensation front (at $\gtrsim 10$ -30 AU; Bergin 2009; Dodson-Robinson et al. 2009), resulting in oxygen-enriched solids and carbon-enriched gas in the region between the H₂O and CO condensation fronts. Some additional volatile elements can be trapped in clathrate hydrates within this region of the disk (Lunine & Stevenson 1985), but as these materials are also water-rich, the solids between the H₂O and CO condensation fronts are expected to be enriched in oxygen and depleted in carbon relative to bulk nebular values (Hersant et al. 2001). Therefore, the addition of accreted planetesimals from this region of the disk would be expected to *decrease* the C/O ratio of a giant planet’s atmosphere below the stellar ratio (e.g., Gautier et al. 2001; Hersant et al. 2004). In contrast, Lodders (2004) suggests that disks also contain a “tar line” inward of the snow line, where refractory organics are stable but water ice has evaporated. If a carbon-rich giant planet gets its extra carbon from solid material, then it is likely from Lodders’ tarry solids or from some kind of carbon-rich refractory phase that remains in the inner solar system after the ice has evaporated (e.g., Ebel & Alexander 2011). This scenario suggests that the carbon-rich giant planet would have to have accreted these solids during or after migration into the inner solar system.

Note that if the planet were to accrete greatly enhanced silicate or metal abundances, a potentially greater fraction of the oxygen could be tied up in condensed silicates and oxides in these planets, leaving the atmosphere above these condensate clouds to be oxygen-depleted. However, silicate and metal condensates in the protoplanetary disk are typically already saturated with oxygen (i.e., metal oxides and silicates like MgSiO₃ and Mg₂SiO₄), making it unlikely that the accretion of metals and silicates in excess of solar proportions would be a mechanism for depleting oxygen in the planets.

In another scenario, the carbon enrichment in a giant planet could result from accreted gas rather than from solids. Öberg et al. (2011) suggest that planets like WASP-12b could have formed beyond the H₂O snow line, with the C/O enhancement simply resulting from the enhanced gas-phase nebular C/O ratio that results from H₂O condensation. For that scenario to work, there cannot be much mixing between the protoplanetary core (which is presumably water-rich due the planet’s formation region beyond the snow line) and the atmosphere after the planet undergoes its fast runaway gas-accretion phase. Moreover, the planet cannot continue to accrete large quantities of more oxygen-rich gas as it migrates to its present position close to its host star, and it cannot accrete a late veneer of oxygen-rich solids that would bring its C/O ratio back to the bulk nebular value. If the planet becomes massive enough early on to create a gap in the disk around its orbit, then Type II migration could ensue (Ward 1997); because the creation of the gap can substantially slow down the rate at which the planet accretes gas (D’Angelo & Lubow 2008), continued gas accretion may not be much of a factor for these planets once they begin migrating. Accretion of solids could still be important, but the current orbital positions of the transiting planets lie well within the condensation fronts for things like silicate and metals within the protoplanetary disk, and evaporation of most

condensates might prevent these planets from accreting significant quantities of solids once the planets become parked at their present orbits. One observational consequence of this scenario would be a planetary metallicity the same order as the host star (Öberg et al. 2011), as superstellar metallicities would imply a larger contribution from solids (unless photoevaporation of the disk is responsible for enhancing virtually all heavy elements in the protoplanetary disk, see Guillot & Hueso 2006). With this scenario, one would expect C/O ratios near unity, as CO is by far the dominant carbon- and oxygen-bearing gas in the region between the H₂O and CO condensation fronts; note that CO₂ seems to be less important in a column-integrated sense than Öberg et al. (2011) have assumed (see, e.g., Willacy & Langer 2000; Willacy & Woods 2009; Walsh et al. 2012).

There is one other region of the protoplanetary disk in which the gas-phase abundance of CO is expected to significantly exceed that of water (even assuming bulk solar C/O ratios), and that is in the very inner regions of the disk ($\lesssim 0.1$ AU) where high temperatures (> 1800 K) begin to affect the stability of water. Water thermally dissociates at about 2500 K, whereas CO can survive to ~ 4000 K (e.g., Najita et al. 2007). Excess oxygen not tied up in CO would be present as O and O⁺ in these regions and might be expected to have different vertical distributions than CO due to molecular and ambipolar diffusion, with O and O⁺ being concentrated at higher altitudes in the disk atmosphere than CO. At these high altitudes, the O and O⁺ might be more vulnerable to loss processes like stellar-wind stripping (Matsuyama et al. 2009) or accelerated accretion onto the star (Elmegreen 1978). As such, the gas near the mid-plane could be carbon-rich in these warm inner-disk regions, with CO the dominant carbon and oxygen constituent. Disk-chemistry models do not generally extend to regions so near the star, but observations of CO overtone emission in young low-mass stellar objects suggests that the CO emission derives from the ~ 0.05 – 0.3 AU region (Chandler et al. 1993; Najita et al. 2000). Observations of CO and H₂O emission obtained for the same disk are consistent with the CO being located inward of, and at higher temperatures than, the H₂O (Carr et al. 2004; Thi & Bik 2005). Since hot Jupiters end up in these inner-disk regions after whatever migration process gets them there, local accretion of gas may also account for high atmospheric C/O ratios. Again, since gas accretion is the culprit for the high C/O ratio in this scenario, one might expect the planet’s metallicity to be similar to the host star’s, unless H has been preferentially lost in the nebula (Guillot & Hueso 2006). Another potential observational test for this scenario would be the N/O ratio, as N₂ would be the only other stable heavy molecule abundant under these conditions.

The fact that we derive C/O ratios near unity for three out of four of the hot Jupiters investigated in this paper (and the fourth might also be just below 1) seems to suggest that the CO-rich gas accretion scenarios from either the hot inner nebula or from beyond the H₂O snow line (e.g., Öberg et al. 2011) represent the most likely explanation for the atmospheric carbon enrichment, as the carbon-rich-solid accretion scenario could potentially lead to $C/O \gg 1$. However, for carbon-rich atmospheres,

graphite is expected to be a major condensate under temperature-pressure conditions in extrasolar giant planets, and graphite would thus commandeer the excess available carbon, leaving $C/O = 1$ above the graphite clouds (e.g., Lodders & Fegley 1997). The carbon-rich-solid scenario is therefore still a viable option, even for planets with an apparent $C \approx O$. Note, however, that WASP-12b is too hot for graphite to form, and if the atmosphere had a C/O ratio much greater than 1, we would expect to see spectral evidence to that effect.

Our own giant planets do not shed much light on the likelihood of these scenarios. The overall enhanced metallicity for Jupiter and the other giant planets suggests that solid planetesimals were instrumental in supplying heavy elements to our own solar-system giant planets (e.g., Owen et al. 1999). However, the ultimate cause of the near-equal enrichments of most heavy elements measured by the *Galileo* probe is under debate (Niemann et al. 1998; Wong et al. 2004; Owen et al. 1999; Gautier et al. 2001; Lodders 2004; Owen & Encrenaz 2006; Hersant et al. 2004; Alibert et al. 2005; Guillot & Hueso 2006; Mousis et al. 2009b). The fact that the probe entered a dry hot-spot region on Jupiter and was not able to measure the deep water abundance is unfortunate, as the O/H enhancement over solar (or lack thereof) could have helped distinguish between different formation scenarios (e.g., Lunine et al. 2004; Atreya & Wong 2005). Indirect evidence based on the observed CO abundance and disequilibrium-chemistry arguments is uncertain enough that a range of bulk Jovian C/O ratios is possible from these calculations (cf. Fegley & Lodders 1994; Lodders & Fegley 2002; Bézard et al. 2002; Visscher et al. 2010b), although the latest models seem to favor C/O ratios \gtrsim solar on Jupiter (Visscher & Moses 2011), seeming to select against some of the high-water-ice and high-clathrate accretion scenarios. Given that Jupiter and transiting planets had very different migration histories, it is not clear that their carbon and oxygen inventories would have come from a similar source.

In any case, the C/O ratio and bulk metallicity within a giant planet’s atmosphere provide important clues that may help us unravel the puzzle of giant planet formation and evolution. Further investigations that can constrain these properties from transit and eclipse observations are warranted. Ultimately, it will be important to collect a statistically significant sample of exoplanet atmospheric properties to determine how common carbon-rich giant planets are within the exoplanet population.

6. SUMMARY

Analyses of transit and eclipse observations suggest that some transiting extrasolar giant planets have unexpectedly low H₂O abundances (e.g., Seager et al. 2005; Richardson et al. 2007; Grillmair et al. 2007; Swain et al. 2009a,b; Madhusudhan & Seager 2009, 2010a; Désert et al. 2009; Sing et al. 2009; Line et al. 2011b; Lee et al. 2012; Cowan et al. 2012; Madhusudhan 2012). Atmospheres with solar-like elemental abundances in thermochemical equilibrium are expected to have abundant water (e.g., Lodders & Fegley 2002), and disequilibrium processes like photochemistry cannot seem to deplete water sufficiently in the infrared pho-

ospheres of these planets to explain the observations (e.g., see Section 3; Line et al. 2010; Moses et al. 2011). While aerosol extinction might help explain the lack of water-absorption signatures in some of the near-infrared transit observations (Lecavelier des Etangs et al. 2008; Pont et al. 2008; Sing et al. 2009, 2011; Gibson et al. 2012), scattering and absorption from clouds or hazes should be less of a factor for the mid-infrared secondary-eclipse observations, unless the clouds are optically thick in the vertical, contain relatively large particles, and are located at pressure levels within the infrared photosphere (e.g., Liou 2002). Such conditions may not be met for the cooler transiting planets like HD 189733b, TrES-1, or XO-1b, where major cloud-forming species like iron or magnesium silicates will condense too deep to affect the secondary-eclipse spectra (Fortney et al. 2005, 2006b, 2010), or for the hottest hot Jupiters like WASP-12b, where temperatures remain so hot throughout the column that iron and silicates will not condense. Extinction from clouds is therefore not expected to be the culprit for the low derived water abundances from thermal-infrared secondary-eclipse observations of many exoplanets, and if the interpretation is robust, we must look to other potential sources for the observed behavior.

A low water abundance is a natural consequence of an atmosphere with a C/O ratio of 1 or greater. Motivated by the recent derivation of a carbon-rich atmosphere for WASP-12b based on secondary-eclipse observations (Madhusudhan et al. 2011a), we have examined the influence of the C/O ratio on the composition of extrasolar giant planet atmospheres, both from a thermochemical equilibrium standpoint and as a result of disequilibrium processes like transport-induced quenching and photochemistry. We find that the equilibrium composition of hot Jupiters is very sensitive to the C/O ratio (see also Seager et al. 2005; Kuchner & Seager 2005; Fortney 2005; Lodders 2010; Madhusudhan et al. 2011a,b; Madhusudhan 2012; Kopparapu et al. 2012). Carbon monoxide is a major constituent on all hot Jupiters whose atmospheres reside on the CO side of the CH₄-vs.-CO stability field, regardless of the C/O ratio (at least for the range $0.1 < C/O < 2$), whereas H₂O and CO₂ become significant constituents for C/O < 1, and CH₄, HCN, and C₂H₂ become significant constituents for C/O > 1. Disequilibrium processes do not change this conclusion, although photochemistry can greatly enhance the HCN and C₂H₂ abundances, and transport-induced quenching can enhance the lower-stratospheric abundances of CH₄, NH₃, and HCN, for a variety of assumed C/O ratios (see also Moses et al. 2011; Visscher & Moses 2011). Despite rapid photolytic destruction by the intense incident UV radiation and despite kinetic attack by atomic H, water survives in hot-Jupiter atmospheres due to the efficient recycling processes that occur in an H₂-dominated atmosphere. A low derived water abundance for a transiting hot Jupiter may therefore be indicative of an atmosphere with a C/O ratio greater than solar (see also Madhusudhan et al. 2011a; Madhusudhan 2012).

We compare the results of our thermochemical and photochemical kinetics and transport models with *Spitzer* secondary-eclipse data from WASP-12b, XO-1b, CoRoT-2b, and HD 189733b — four exoplanets whose atmospheres have been described as having potentially low

water abundances (e.g., Madhusudhan & Seager 2009; Madhusudhan et al. 2011a; Madhusudhan 2012). We find that disequilibrium models with C/O ~ 1 are consistent with photometric data from WASP-12b, XO-1b, and CoRoT-2b, confirming the possible carbon-rich nature of these planets. In contrast, spectra from HD 189733b are more consistent with C/O $\lesssim 1$. In particular, our synthetic spectra for HD 189733b compare well with *Spitzer* secondary-eclipse photometric data for models with metallicities between 1-5 \times solar for moderately enhanced C/O ratios between 0.88-1.0. These fits are not unique: the specific derived C/O ratio that provides the best fit to the data will be dependent on the assumed thermal structure and atmospheric metallicity, with lower metallicities and/or higher atmospheric temperatures allowing lower (i.e., more solar-like) C/O ratios to remain consistent with the low inferred water absorption from these planets. In those cases, however, the relative band ratios in the *Spitzer* IRAC channels are not always well reproduced.

Our models indicate that hydrogen cyanide is an important atmospheric opacity source when C/O $\gtrsim 1$, such that HCN can even dominate the opacity in the 3.6 and 8.0 μm *Spitzer* channels for a variety of conditions. For example, we find that HCN is the main absorber in the 3.6 and 8.0 μm bands on the very hot WASP-12b, rather than CH₄ being responsible (as was suggested by Madhusudhan et al. 2011a) or C₂H₂ being responsible (as was suggested by Kopparapu et al. 2012); however, this result could change for different assumptions about the thermal structure and C/O ratio. Acetylene is less important overall for the *Spitzer* bandpasses, but C₂H₂ is an important photochemical product in cooler atmospheres for a variety of C/O ratios and can become a significant equilibrium constituent in hotter atmospheres when C/O > 1.

Carbon dioxide is not a dominant constituent in our equilibrium or disequilibrium models regardless of the C/O ratio (again, for the range $0.1 < C/O < 2$ and near-solar metallicities). A CO₂/H₂O ratio greater than unity for HD 189733b (see Swain et al. 2009a; Madhusudhan & Seager 2009; Line et al. 2011b; Lee et al. 2012) would require a metallicity greater than 2000 \times solar or a C/O ratio $\ll 0.1$, with both scenarios seeming to be inconsistent with the planet's bulk density and secondary-eclipse observations. We therefore cannot explain the relatively large CO₂ abundance inferred from *HST*/NICMOS observations of (Swain et al. 2009a). In general, we do not expect CO₂ to be a major constituent in the atmospheres of near-solar-composition hot Jupiters. Therefore, spectral modelers may want to consider the effects of species like HCN and NH₃ instead of (or in addition to) CO₂ and/or photochemical modelers will need to come up with new mechanisms to explain enhanced CO₂ abundances if spectral features on hot Jupiters can be tied uniquely to CO₂.

Although an atmospheric C/O ratio $\gtrsim 1$ on a giant planet could result from a carbon-enriched protoplanetary disk (e.g., Madhusudhan et al. 2011b), there are also ways in which such a planet could form in a disk that possesses more solar-like bulk elemental ratios. Vapor condensation within the protoplanetary disk is one significant way in which elements can be fractionated, with the solids and vapor ending up with very different C/O

ratios. Carbon-rich giant planets could have accreted water-ice-poor, carbon-rich solids during their migration through the disk regions inward of the snow line (e.g., Lodders 2004; Ebel & Alexander 2011), or they could get their carbon enrichment from the accretion of CO-rich, H₂O-poor gas, either during the runaway accretion phase as they formed in the region between the water and CO condensation fronts in the outer disk (e.g., Öberg et al. 2011) or *in situ* from the inner disk once their migration stopped very close to the host star. Regardless of whether these specific scenarios are viable or not, the atmospheric C/O ratio and bulk metallicity provide im-

portant clues regarding the formation and evolution of giant planets, and it is hoped that future spectral observations can reveal how common carbon-rich giant planets are within the exoplanet population.

We thank Mark Marley and Jonathan Fortney for interesting exoplanet science discussions. The first author (JM) gratefully acknowledges support from the NASA Planetary Atmospheres Program grant number NNX11AD64G, CV acknowledges support from NNX10AF64G, and NM acknowledges support from the Yale Center of Astronomy and Astrophysics through a YCAA Postdoctoral Fellowship.

REFERENCES

- Alibert, Y., Mousis, O., & Benz, W. 2005, *ApJ*, 622, L145
 Allen, M., Yung, Y. L., & Waters, J. W. 1981, *J. Geophys. Res.*, 86, 3617
 Allende Prieto, C., Barklem, P. S., Asplund, M., Ruiz Cobo, B. 2001, *ApJ*, 558, 830
 Allende Prieto, C., Lambert, D. L., & Asplund, M. 2002, *ApJ*, 573, L137
 Alonso, R., Auvergne, M., Baglin, A., et al. 2008, *A&A*, 482, L21
 Alonso, R., Deeg, H. J., Kabath, P., & Rabus, M. 2010, *ApJ*, 139, 1481
 Asplund, M., Grevesse, N., & Sauval, A. J. 2005, in *Cosmic Abundances as Records of Stellar Evolution and Nucleosynthesis in honor of David L. Lambert*, ed. T. G. Barnes III and F. N. Bash, ASP Conference Series, Vol. 336, (San Francisco: Astronomical Society of the Pacific), 25
 Asplund, M., Grevesse, N., Sauval, A. J., & Scott, P. 2009, *Ann. Rev. Astron. Astrophys.*, 47, 481
 Atreya, S. K., & Wong, A.-H. 2005, *Space Sci. Rev.*, 116, 121
 Atreya, S. K., Wong, M. H., Owen, T. C., et al. 1999, *Planet. Space Sci.*, 47, 1243
 Ayers, T. 2005, in *Proc. 13th Cool Stars Workshop*, ed. F. Favata, G. Hussain, & B. Batrick, ESA SP-560, 419
 Barman, T. 2007, *ApJ*, 661, L191
 Barman, T. 2008, *ApJ*, 676, L61
 Barman, T. S., Hauschildt, P.H., & Allard, F. 2005, *ApJ*, 632, 1132
 Beaulieu, J. P., Carey, S., Ribas, I., & Tinetti, G. 2008, *ApJ*, 677, 1343
 Beaulieu, J. P., Kipping, D. M., Batista, V., et al. 2010, *MNRAS*, 409, 963
 Bergin, E. 2009, arXiv:0908.3708
 Bézard, B., Lellouch, E., Strobel, D., Maillard, J.-P., Drossart, P. 2002, *Icarus*, 159, 95
 Borysow, A. 2002, *A&A*, 390, 779
 Borysow, A., Jorgensen, U. G., & Zheng, C. 1997, *A&A*, 324, 185
 Bond, J. C., O'Brien, D. P., & Loretta, D. S. 2010, *ApJ*, 715, 1050
 Bouchy, F., Udry, S., Mayor, M., et al. 2005, *A&A*, 444, L15
 Bouchy, F., Queloz, D., Deleuil, M., et al. 2008, *A&A*, 482, L25
 Burcat, A., & Ruscic, B. 2005, *Third Millennium Ideal and Condensed Phase Thermochemical Database for Combustion with Updates from Active Thermochemical Tables*, TAE 960, ANL-05/20 (Argonne, IL; Argonne National Laboratory)
 Burrows, A., & Orton, G. 2010, in *Exoplanets*, ed. S. Seager (Tucson, AZ: Univ. Arizona Press), 419.
 Burrows, A., & Sharp, C. M. 1999, *ApJ*, 512, 843
 Burrows, A., Hubeny, I., & Sudarsky, D. 2005, *ApJ*, 625, L135
 Burrows, A., Sudarsky, D., & Hubeny, I. 2006, *ApJ*, 650, 1140
 Burrows, A., Hubeny, I., Budaj, J., Knutson, H. A., & Charbonneau, D., 2007, *ApJ*, 668, L171
 Burrows, A., Budaj, J., & Hubeny, I., 2008, *ApJ*, 678, 1436
 Caffau, E., Ludwig, H.-G., Steffen, M., et al. 2008, *A&A*, 488, 1031
 Caffau, E., Ludwig, H.-G., Bonifacio, P., et al. 2010, *A&A*, 514, A92
 Campo, C. J., Harrington, J., Hardy, R. A., et al. 2011, *ApJ*, 727, 125
 Carr, J. S., Tokunaga, A. P., & Najita, J. R. 2004, *ApJ*, 603, 213
 Castelli, F., & Kurucz, R. L., 2004, arXiv:astro-ph/0405087v1
 Chandler, C. J., Carlstrom, J. E., Scoville, N. Z., Dent, W. R. F., & Geballe, T. R. 1993, *ApJ*, 412, L71
 Charbonneau, D., Allen, L. E., Megeath, S. T., et al. 2005, *ApJ*, 626, 523
 Charbonneau, D., Knutson, H. A., Barman, T., et al. 2008, *ApJ*, 686, 1341
 Chase, M. W. 1998, *NIST-JANAF Thermochemical Tables*, 4th ed., *J. Phys. Chem. Ref. Data*, 28, Monograph No. 9 (Melville, NY: AIP)
 Christiansen, J. L., Ballard, S., Charbonneau, D., et al. 2010, *ApJ*, 710, 97
 Ciesla, F. J., & Cuzzi, J. N. 2006, *Icarus*, 181, 178
 Cooper, C. S., & Showman, A. P., 2006, *ApJ*, 649, 1048
 Cowan, N. B., & Agol, E. 2011, *ApJ*, 729, 54
 Cowan, N. B., Machalek, P., Croll, B., et al. 2012, *ApJ*, 747, 82
 Croll, B., Lafreniere, D., Albert, L., et al. 2011, *AJ*, 141, 30
 Cuzzi, J. N., & Zahnle, K. J. 2004, *ApJ*, 614, 490
 Cuzzi, J. N., Ciesla, F. J., Petaev, M. I., Krot, A. N., Scott, E. R. D., & Weidenschilling, S. J. 2005, in *Chondrites and the Protoplanetary Disk*, ed. A. N. Krot, E. R. D. Scott, & B. Reipurth, ASP Conference Series, Vol. 341, (San Francisco: Astronomical Society of the Pacific), 732
 Cyr, K. E., Sears, W. D., & Lunine, J. I. 1998, *Icarus*, 135, 537
 Cyr, K. E., Sharp, C. M., & Lunine, J. I. 1999, *J. Geophys. Res.*, 104, 19003
 D'Angelo, G., Lubow, S. H. 2008, *ApJ*, 685, 560
 Delgado Mena, E., Israelian, G., González Hernández, J. I., et al. 2010, *ApJ*, 725, 2349
 Deming, D., Knutson, H., Agol, E., et al., 2011, *ApJ*, 726, 95
 Désert, J.-M., Lecavelier des Etangs, A., Hébrard, G., et al. 2009, *ApJ*, 699, 478
 Dodson-Robinson, S. E., Willacy, K., Bodenheimer, P., Turner, N. J., & Beichman, C. A. 2009, *Icarus*, 200, 672
 Ebel, D. S., & Alexander, C. M. O'D. 2011, *Planet. Space Sci.*, 59, 1888
 Ecuivillon, A., Israelian, G., Santos, N. C., et al. 2004, *A&A*, 426, 619
 Ecuivillon, A., Israelian, G., Santos, N. C., et al. 2006, *A&A*, 445, 633
 Elmegreen, B. G. 1978, *Moon Planets*, 19, 261
 Fegley, B., Jr., & Lodders, K. 1994, *Icarus*, 110, 117
 Fortney, J. J. 2005, *MNRAS*, 364, 649
 Fortney, J. J. 2012, *ApJ*, 747, L27
 Fortney, J. J., & Marley, M. S. 2007, *ApJ*, 666, L45
 Fortney, J. J., Marley, M. S., Lodders, K., Saumon, D., & Freedman, R. 2005, *ApJ*, 627, L69
 Fortney, J. J., Cooper, C. S., Showman, A. P., Marley, M. S., & Freedman, R. S. 2006a, *ApJ*, 652, 746
 Fortney, J. J., Saumon, D., Marley, M. S., Lodders, K., & Freedman, R. S. 2006b, *ApJ*, 642, 495
 Fortney, J. J., Lodders, K., Marley, M. S., & Freedman, R. S. 2008a, *ApJ*, 678, 1419
 Fortney, J. J., Marley, M. S., Saumon, D., Lodders, K. 2008b, *ApJ*, 683, 1104
 Fortney, J. J., Shabram, M., Showman, A. P., et al. 2010, *ApJ*, 709, 1396

- Freedman, R. S., Marley, M. S., & Lodders, K. 2008, *ApJS*, 174, 504
- Gaidos, E. J. 2000, *Icarus*, 145, 637
- García Muñoz, A. 2007, *Planet. Space Sci.*, 55, 1426
- Gautier, D., Hersant, F., Mousis, O., & Lunine, J. I. 2001, *ApJ*, 550, L227; Erratum: *ApJ*, 559, L183
- Gibson, N. P., Aigrain, S., Pont, F., et al. 2012, *MNRAS*, in press, arXiv:1201.6573.
- Gillon, M., Lanotte, A. A., Barman, T., et al. 2010, *A&A*, 511, A3
- Gladstone, G. R., Allen, M., & Yung, Y. L. 1996, *Icarus*, 119, 1
- Gordon, S., & McBride, B. J. 1994, *NASA Reference Publ.* 1311
- Grevesse, N., Asplund, M., & Sauval, A. J. 2007, *Space Sci. Rev.*, 130, 105
- Grevesse, N., Asplund, M., Sauval, A. J., & Scott, P. 2010, *Astrophys. Space Sci.*, 328, 179
- Grillmair, C. J., Charbonneau, D., Burrows, A., et al. 2007, *ApJ*, 658, L115
- Grillmair, C. J., Burrows, A., Charbonneau, D., et al. 2008, *Nature*, 456, 767
- Guillot, T., & Hueso, R. 2006, *MNRAS*, 367, L47
- Guillot, T., & Havel, M. 2011, *A&A*, 527, A20
- Gurvich, L. V., Veyts, I. V., & Alcock, C. B. 1998-1994, *Thermodynamic Properties of Individual Substances*, 3 vols. (4th ed., New York: Hemisphere Publishing)
- Harris, G. L., Lerner, F. C., Tennyson, J., Kaminsky, B. M., Pavlenko, Y. V., & Jones, H. R. A. 2008, *MNRAS*, 390, 143
- Hebb, L., Collier-Cameron, A., Loeillet, B., et al. 2009, *ApJ*, 693, 1920
- Hersant, F., Gautier, D., & Huré, J.-M. 2001, *ApJ*, 554, 391
- Hersant, F., Gautier, D., & Lunine, J. I. 2004, *Planet. Space Sci.*, 52, 623
- Hersant, F., Gautier, D., Tobie, G., & Lunine, J. I. 2008, *Planet. Space Sci.*, 56, 1103
- Hubeny, I., & Burrows, A. 2007, *ApJ*, 669, 1248
- Hubeny, I., Burrows, A., & Sudarsky, D., 2003, *ApJ*, 594, 1011
- Huitson, C.M., Sing, D.K., Vidal-Madjar, A., et al., 2012, *MNRAS*, 422, 2477
- Hutson, M., & Ruzicka, A., 2000, *Meteorit. Planet. Sci.*, 35, 601
- Iro, N., Bézard, B., & Guillot, T. 2005, *A&A*, 436, 719
- Jacquinet-Husson, N., Scott, N. A., Chédin, A., et al. 2008, *JQSRT*, 109, 1043
- Johnson, T. V., & Estrada, P. R. 2009, in *Saturn from Cassini-Huygens*, ed. M. K. Dougherty, L. W. Esposito, & S. M. Krimigis (Dordrecht: Springer), 55
- Knutson, H. A., Charbonneau, D., Allen, L. E., et al. 2007, *Nature*, 447, 183
- Knutson, H. A., Charbonneau, D., Allen, L. E., Burrows, A., & Megeath, S. E. 2008, *ApJ*, 673, 526
- Knutson, H. A., Charbonneau, D., Burrows, A., O'Donovan, F. T., & Mandushev, G. 2009a, *ApJ*, 691, 866
- Knutson, H. A., Charbonneau, D., Cowan, N. B., et al. 2009b, *ApJ*, 690, 822
- Knutson, H. A., Howard, A. W., & Isaacson, H. 2010, *ApJ*, 720, 1569
- Knutson, H. A., Madhusudhan, N., Cowan, N. B., et al. 2011, *ApJ*, 735, 27
- Knutson, H. A., Lewis, N., Fortney, J. J., et al. 2012, *ApJ*, 754, 22
- Kopparapu, R. K., Kasting, J. F., & Zahnle, K. J. 2012, *ApJ*, 745, 77
- Koskinen, T. T., Aylward, A. D., Smith, C. G. A., & Miller, S. 2007, *ApJ*, 661, 515
- Koskinen, T. T., Yelle, R. V., Lavvas, P., & Lewis, N. K. 2010, *ApJ*, 723, 116
- Krot, A. N., Fegley, B., Jr., Lodders, K., & Palme, H. 2000, in *Protostars and Planets IV*, ed. Mannings, V., Boss, A. P., & Russell, S. S., (Tucson: University of Arizona Press), 1019
- Kuchner, M. J., & Seager, S. 2005, arXiv:astro-ph/0504214
- Larimer, J. W. 1975, *Geochim. Cosmochim. Acta*, 39, 389
- Larimer, J. W., & Bartholomay, M. 1979, *Geochim. Cosmochim. Acta*, 43, 1455
- Lattimer, J. M., Schramm, D. N., & Grossman, L. 1978, *ApJ*, 219, 230
- Lecavelier des Etangs, A., Pont, F., Vidal-Madjar, A., & Sing, D. 2008, *A&A*, 481, L83
- Lee, J.-M., Fletcher, L.N., & Irwin, P.G.J. 2011, *MNRAS*, 420, 170
- Lewis, J. S., & Fegley, B., Jr. 1984, *Space Sci. Rev.*, 39, 163
- Liang, M.-C., Parkinson, C. D., Lee, A. Y. T., Yung, Y. L., & Seager, S. 2003, *ApJ*, 596, L247
- Liang, M.-C., Seager, S., Parkinson, C. D., Lee, A. Y. T., & Yung, Y. L. 2004, *ApJ*, 605, L61
- Line, M. R., Liang, M. C., & Yung, Y. L. 2010, *ApJ*, 717, 496
- Line, M. R., Vasisth, G., Chen, P., Angerhausen, D., & Yung, Y. L. 2011a, *ApJ*, 738, 32
- Line, M. R., Zhang, X., Vasisth, G., Natraj, V., Chen, P., & Yung, Y. L. 2011b, arXiv:1111.2612v1
- Liou, K. N. 2002, *An Introduction to Atmospheric Radiation*, (2nd ed., Amsterdam: Academic Press)
- Lodders, K. 2002, *ApJ*, 577, 974
- Lodders, K. 2004, *ApJ*, 611, 587
- Lodders, K. 2010, in *Formation and Evolution of Exoplanets*, ed. R. Barnes (Berlin: Wiley), 157
- Lodders, K., & Fegley, B., Jr. 1993, *Meteoritics*, 28, 387
- Lodders, K., & Fegley, B., Jr. 1995, *Meteoritics*, 30, 661
- Lodders, K., & Fegley, B., Jr. 1997, *AIP Conf. Proc.*, 402, 391
- Lodders, K., & Fegley, B., Jr. 1999, in *Asymptotic Giant Branch Stars*, ed. T. Le Bertre, A. Lebre, and C. Waelkens, IAU Symposium #191, 279
- Lodders, K., & Fegley, B., Jr. 2002, *Icarus*, 155, 393
- Lodders, K., Palme, H., & Gail, H.-P. 2009, in *The Solar System*, Landolt-Börnstein, New Series, Vol. VI/4B, ed. J. E. Trümper, (Berlin:Springer-Verlag), 560
- Lunine, J. I., & Stevenson, D. J. 1985, *ApJS*, 58, 493
- Lunine, J. I., Coradini, A., Gautier, D., Owen, T. C., & Wuchterl, G. 2004, in *Jupiter: The Planet, Satellites & Magnetosphere*, ed. F. Bagenal, T. E. Dowling, & W. B. McKinnon (Cambridge: Cambridge Univ. Press), 19
- Machalek, P., McCullough, P. R., Burke, C. J., Valenti, J. A., Burrows, A., & Hora, J. L. 2008, *ApJ*, 684, 1427
- Madhusudhan, N. 2012, *ApJ*, 758, 36
- Madhusudhan, N., & Seager, S. 2009, *ApJ*, 707, 24
- Madhusudhan, N., & Seager, S. 2010a, *ApJ*, 725, 261
- Madhusudhan, N., & Seager, S. 2011, *ApJ*, 729, 41
- Madhusudhan, N., et al. 2011a, *Nature*, 469, 64
- Madhusudhan, N., Mousis, O., Johnson, T.V., & Lunine, J.I. 2011b, *ApJ*, 743, 191
- Marley, M. S., Fortney, J. J., Seager, S., & Barman, T. 2007, in *Protostars and Planets V*, ed. B. Reipurth, D. Jewitt, & K. Keil (Tucson, AZ: Univ. Arizona Press), 733
- Matsuyama, I., Johnstone, D., & Hollenbach, D. 2009, *ApJ*, 700, 10
- McCullough, P. R., Stys, J. E., Valenti, J. A., et al. 2006, *ApJ*, 648, 1228
- Michelangeli, D. V., Allen, M., Yung, Y. L., Shia, R.-L., Crisp, D., & Eluszkiewicz, J. 1992, *J. Geophys. Res.*, 97, 865
- Miller-Ricci Kempton, E., Zahnle, K., & Fortney, J. J. 2012, *ApJ*, 745, 3
- Mizuno, H., Nakazawa, K., & Hayashi, C. 1978, *Prog. Theor. Phys.*, 60, 699
- Moses, J. I., Visscher, C. 2011, EPSC-DPS Joint Meeting, held 2-7 October 2011, Nantes, France, 1634 2011 September 11-17, abstract #40.04
- Moses, J. I., Bézard, B., Lellouch, E., et al. 2000a, *Icarus*, 143, 244
- Moses, J. I., Lellouch, E., Bézard, B., et al. 2000b, *Icarus*, 145, 166
- Moses, J. I., Fouchet, T., Bézard, B., et al. 2005, *J. Geophys. Res.*, 110, E08001
- Moses, J. I., Visscher, C., Keane, T. C., & Sperier, A. 2010, *Faraday Disc.*, 147, 103
- Moses, J. I., Visscher, C., Fortney, J. J., et al. 2011, *ApJ*, 737, 15
- Mousis, O., Lunine, J. I., Tinetti, G., et al. 2009a, *A&A*, 507, 1671
- Mousis, O., Marboeuf, U., Lunine, J. I., et al. 2009b, *ApJ*, 696, 1348
- Mousis, O., Lunine, J. I., Petit, J.-M., et al. 2011, *ApJ*, 727, 77
- Najita, J. R., Edwards, S., Basri, G., & Carr, J. 2000, in *Protostars and Planets IV*, eds. V. Mannings, A. P. Boss, & S. Russell (Tucson, AZ: Univ. Arizona Press), 457
- Najita, J. R., Carr, J. S., Glassgold, A. E., & Valenti, J. A. 2007, in *Protostars and Planets V*, ed. B. Reipurth, D. Jewitt, & K. Keil (Tucson, AZ: Univ. Arizona Press), 507
- Najita, J. S., Ádámkóvics, M., & Glassgold, A. E. 2011, *ApJ*, 743, 147
- Niemann, H. B., Atreya, S. K., Carignan, G. R., et al. 1998, *J. Geophys. Res.*, 103, 22831

- Öberg, K. I., Murray-Clay, R., & Bergin, E. A. 2011, *ApJ*, 743, L16
- Owen, T., & Encrenaz, T. 2006, *Planet. Space Sci.*, 54, 1188
- Owen, T., Mahaffy, P., Niemann, H. B., et al. 1999, *Nature*, 402, 269
- Pasek, M. A., Milsom, J. A., Ciesla, F. J., et al. 2005, *EPSL*, 101, 180
- Petaev, M. I., & Wood, J. A. 2005, in *Chondrites and the Protoplanetary Disk*, ed. A. N. Krot, E. R. D. Scott, & B. Reipurth, ASP Conference Series, Vol. 341, (San Francisco: Astronomical Society of the Pacific), 373
- Petigura, E. A., & Marcy, G. W. 2011, *ApJ*, 735, 41
- Pollack, J. B., Hubickyj, O., Bodenheimer, P., et al. 1996, *Icarus*, 124, 62
- Pont, F., Knutson, H., Gilliland, R. L., Moutou, C., & Charbonneau, D. 2008, *MNRAS*, 385, 109
- Prinn, R. G., & Barshay, S. S. 1977, *Science*, 198, 1031
- Prinn, R. G., & Fegley, B., Jr. 1989, in *Origin and Evolution of Planetary and Satellite Atmospheres*, ed. S. K. Atreya, J. B. Pollack, M. S. Matthews, (Tucson: Univ. Arizona Press), 78
- Richardson, L. J., Deming, D., Horning, K., Seager, S., & Harrington, J. 2007, *Nature*, 445, 892
- Rothman, L. S., Jacquemart, D., Barbe, A., et al. 2005, *JQSRT*, 96, 139
- Rothman, L. S., Gordon, I. E., Barbe, A., et al. 2009, *JQSRT*, 110, 533
- Seager, S., & Sasselov, D. D. 1998, *ApJ*, 502, L157
- Seager, S., Richardson, L. J., Hansen, B. M. S., et al. 2005, *ApJ*, 632, 1122
- Seager, S., & Deming, D. 2010, *Ann. Rev. Astron. Astrophys.*, 48, 631
- Shabram, M., Fortney, J. J., Greene, T. P., & Freedman, R. S. 2011, *ApJ*, 727, 65
- Sharp, C. M., & Burrows, A. 2007, *ApJS*, 168, 140
- Showman, A. P., Fortney, J. J., Lian, Y., et al. 2009, *ApJ*, 699, 564
- Showman, A. P., Cho, J. Y.-K., & Menou, K. 2010, in *Exoplanets*, ed. S. Seager (Tucson, AZ: Univ Arizona Press), 471.
- Sing, D. K., Désert, J.-M., Lecavelier des Etangs, A., et al. 2009, *A&A*, 505, 891
- Sing, D. K., Pont, F., Aigrain, S., et al. 2011b, *MNRAS*, 416, 1443
- Snellen, I. A. G., de Kok, R. J., de Mooij, E. J. W., & Albrecht, S. 2010a, *Nature*, 465, 1049
- Spiegel, D. S., & Burrows, A. 2010, *ApJ*, 722, 871
- Spiegel, D. S., Silverio, K., & Burrows, A. 2009, *ApJ*, 699, 1487
- Stepinski, T. F., & Valageas, P. 1997, *A&A*, 319, 1007
- Stevenson, D. J., & Lunine, J. I. 1988, *Icarus*, 75, 146
- Swain, M. R., 2012, AAS Meeting Abstracts 220, #505.05
- Swain, M. R., Bouwman, J., Akeson, R. L., Lawler, S., & Beichman, C. A. 2008a, *ApJ*, 674, 482
- Swain, M. R., Vasisht, G., & Tinetti, G. 2008b, *Nature*, 452, 329
- Swain, M. R., Vasisht, G., Tinetti, G., et al. 2009a, *ApJ*, 690, L114
- Swain, M. R., Tinetti, G., Vasisht, G., et al. 2009b, *ApJ*, 704, 1616
- Swain, M. R., Deroo, P., Griffith, C. A., et al. 2010, *Nature*, 463, 637
- Swain, M. R., Deroo, P., Tinetti, G., et al. 2012, arXiv:1205.4736
- Thi, W.-F., & Bik, A. 2005, *A&A*, 438, 557
- Tinetti, G., Vidal-Madjar, A., Liang, M.-C., et al. 2007, *Nature*, 448, 169
- Tinetti, G., Deroo, P., Swain, M. R., et al. 2010, *ApJ*, L139
- Tinetti, G., Beaulieu, J.P., Henning, T., et al. 2012, *Experimental Astronomy*, in press
- Venot, O., Hébrard, G., Agúndez, M., et al. 2012, *A&A*, in press
- Visscher, C., & Fegley, B., Jr. 2005, *ApJ*, 623, 1221
- Visscher, C., Lodders, K., & Fegley, B., Jr. 2006, *ApJ*, 648, 1181
- Visscher, C., Lodders, K., & Fegley, B., Jr. 2010a, *ApJ*, 716, 1060
- Visscher, C., Moses, J. I., & Saslow, S. A. 2010b, *Icarus*, 209, 602
- Visscher, C., & Moses, J. I. 2011, *ApJ*, 738, 72
- Waldmann, I. P., Tinetti, G., Drossart, P., et al. 2012, *ApJ*, 744, 35
- Walsh, C., Nomura, H., Millar, T. J., & Aikawa, Y. 2012, *ApJ*, 747, 114
- Ward, W. R. 1997, *ApJ*, 482, L211
- Wattson, R. B., & Rothman, L. S. 1986, *J. Molec. Spectrosc.*, 119, 83
- Willacy, K., & Langer, W. D. 2000, *ApJ*, 544, 903
- Willacy, K., & Woods, P. M. 2009, *ApJ*, 703, 479
- Winn, J. N. 2010, in *Exoplanets*, ed. S. Seager (Tucson, AZ: Univ Arizona Press), 55.
- Wong, M. H., Mahaffy, P. R., Atreya, S. K., Niemann, H. B., & Owen, T. C. 2004, *Icarus*, 171, 153
- Wooden, D. H. 2008, *Space Sci. Rev.*, 138, 75
- Yelle, R. V. 2004, *Icarus*, 170, 167
- Yung, Y. L., Allen, M., & Pinto, J. P. 1984, *ApJS*, 55, 465
- Zahnle, K., Marley, M. S., & Fortney, J. J. 2009a, arXiv:0911.0728v2
- Zahnle, K., Marley, M. S., Freedman, R. S., Lodders, K., & Fortney, J. J. 2009b, *ApJ*, 701, L20